

Geological modeling of the new CHAMP magnetic anomaly maps using a geographical information system technique

K. Hemant

GeoForschungsZentrum, Potsdam, Germany

S. Maus¹

CIRES, University of Colorado, Boulder, Colorado, USA

Received 13 May 2005; accepted 14 September 2005; published 14 December 2005.

[1] Reliable global crustal field anomaly maps produced from magnetic measurements of the CHAMP satellite mission now allow for quantitative geological studies of crustal structure and composition. We have developed a GIS based forward modeling technique to model these anomaly maps. On the basis of the geologic and tectonic maps of the world, laboratory susceptibility values of the occurring rock types, and the seismic thickness of the crust, a vertically integrated susceptibility grid is generated in the GIS system. In addition, a remanent magnetization grid is computed for the oceanic crust using a digital isochron map of the ocean floor and rotation models of the paleoplates. Combining the global VIS and remanent magnetization grids, the vertical magnetic field anomaly is computed at satellite altitude and compared with the corresponding CHAMP magnetic anomaly map. Over the oceans, induced and remanent magnetization explains well the prominent observed anomalies over the Cretaceous quiet zones. We also find a good agreement between predicted and observed anomalies over the continents. Remaining discrepancies between the predicted and observed anomalies can be used to adjust poorly known boundaries and the composition of the buried Precambrian provinces, until the recomputed anomalies fit the observed anomalies. The feasibility of this approach is demonstrated on Greenland, the West African Craton, Bangui in central Africa, and the Kolyma-Omolon Block in Siberia. We conclude that quantitative information on the lateral extent, the composition and the thickness of the lower crust within a Precambrian province can thus be inferred from the new satellite magnetic anomaly maps.

Citation: Hemant, K., and S. Maus (2005), Geological modeling of the new CHAMP magnetic anomaly maps using a geographical information system technique, *J. Geophys. Res.*, 110, B12103, doi:10.1029/2005JB003837.

1. Introduction

[2] Magnetic anomaly maps produced from airborne and shipborne measurements are routinely used in the preparation of geologic and geophysical models of the crust [Blakely *et al.*, 1995]. These surveys concentrate on geologic features less than about 50 km in lateral dimension. However, in past decades there has been increasing interest in studying large-scale anomalies, hundreds of kilometers in extent, that appear in regional compilations of data from airborne surveys. Spatial variations in these long wavelength anomalies reflect variations in magnetic properties and the thickness of the magnetized layers. New insights on the long wavelength anomalies (half wavelength > 250 km) have come with the first satellite crustal magnetic anomaly

maps from Pogo [Regan *et al.*, 1975], Magsat [Langel *et al.*, 1982; Cain *et al.*, 1989; Arkani-Hamed *et al.*, 1994; Ravat *et al.*, 1995; Sabaka *et al.*, 2000] and Ørsted [Olsen *et al.*, 2000]. The accuracy of the earlier global magnetic anomaly maps, however, was limited by either the higher orbital altitude of the satellites (POGO and Ørsted) or inaccuracies in the attitude determination leading to high noise levels in the vector magnetic field components (Magsat). A breakthrough in crustal field accuracy and resolution has been achieved with the new CHAMP satellite data (http://www.gfz-potsdam.de/pb1/op/champ/main_CHAMP.html) [Maus *et al.*, 2002]. Here we interpret MF3 [Maus *et al.*, 2005], a crustal field model prepared by our group using 3 years of CHAMP scalar and vector data.

[3] Early interpretations of satellite crustal anomaly maps over continental regions concentrated on a direct comparison with regional geologic or tectonic maps [Frey, 1982; Achache *et al.*, 1987]. These studies showed that large-scale features such as shields, cratons and subduction zones are associated with positive anomalies (as caused by enhanced susceptibility) while basins and abyssal plains

¹Also at National Geophysical Data Center, NOAA, Boulder, Colorado, USA.

are associated with negative anomalies. They attributed the negative anomalies to crustal thinning associated with an elevated Curie isotherm and vice versa for the positive anomalies.

[4] Interpretations of the global crustal field anomaly maps have employed forward modeling methods [Meyer *et al.*, 1983; Hahn *et al.*, 1984] as well as the inverse method of Purucker *et al.* [1998]. Because of the nonuniqueness of the magnetic inverse problem, in particular with the longest wavelengths being masked by the main field, all workers used additional information to construct their initial global crustal models. In the model of Meyer *et al.* [1983] and Hahn *et al.* [1984], the crust was classified into 16 crustal types. The classification was based on surface geology and seismic crustal thickness. The model comprised two or three layers. Layer classification, with magnetization in amperes per meter in a 50,000 nT inducing field in brackets, were as follows: sea water (0), sediments (0), upper oceanic layer (1.0), upper continental layer (1.0–2.0), lower crustal layer (0.5), intermediate crustal layer (1.2), and sub-Moho (0). Assuming only induced magnetization as the source of the anomalies, their comparison of the predicted with observed anomalies showed some local agreement with the Magsat derived anomaly map [Langel *et al.*, 1982], but in general, the results were largely in disagreement with the observations. Purucker *et al.* [1998] derived an a priori magnetization distribution model for both continents and oceans, termed “Standard Earth Magnetization Model,” or SEMM-0. Induced magnetization was based on the tectonic classification and crustal thickness of the 3SMAC model [Nataf and Ricard, 1996], while the remanent magnetization was predicted from the global oceanic model of Dyment and Arkani-Hamed [1998]. Using a least squares inverse method, an equivalent source magnetization model (SEMM) was derived by modifying the initial a priori model SEMM-0 until the resulting anomaly pattern matched a Magsat-derived magnetic anomaly map. Recently, this model has been extended to include the sediment thickness given by Laske and Masters [1997], and typical heat flow associated with the tectonic classes [Purucker *et al.*, 2002]. In an alternative approach, Whaler [2003] has inverted the CHAMP crustal anomaly map, finding a crustal magnetization without prior geological assumptions by minimizing the root-mean-square amplitude of the crustal magnetization.

[5] While the effect of induced magnetization is dominant over the continents, magnetic anomalies over the oceans are due both to induced and remanent magnetization. Over subduction zones [Clark *et al.*, 1985; Counil and Achache, 1987] and oceanic plateaus [Frey, 1985; Toft and Arkani-Hamed, 1992; Fullerton *et al.*, 1994; Cohen and Achache, 1994] observed anomalies have been explained in terms of induced magnetization alone. On the other hand, anomalies over the Cretaceous quiet zones (KQZ) and other oceanic anomalies parallel to the mid-oceanic ridges in the North Atlantic [LaBrecque and Raymond, 1985], central Atlantic [Hayling and Harrison, 1986; Purucker and Dyment, 2000], South Atlantic [Purucker and Dyment, 2000], Pacific [Toft and Arkani-Hamed, 1992], eastern Indian Ocean [Taylor, 1991], and southwest Indian Ocean [Fullerton *et al.*, 1994] have been explained in terms of remanent magnetization. The anomalies predicted from the global

oceanic model of Dyment and Arkani-Hamed [1998] show prominent features associated with these KQZs. The sources for the observed anomalies could possibly extend into the upper oceanic mantle [Arkani-Hamed and Strangway, 1986; Arkani-Hamed, 1991].

[6] This paper introduces a geographical information system (GIS) based forward modeling method that is used to derive a global magnetization model based on geological units of the continents and oceans, their respective rock types and a global seismic crustal model. In contrast to the predictive global models of Hahn *et al.* [1984] and Purucker *et al.* [1998], which assign a constant susceptibility to a limited number of geological classes, the global magnetization model derived here has a unique susceptibility value for each geological region of the world, depending on the dominant rock types. Similar to the model of Purucker *et al.* [1998], a remanent magnetization is modeled for the oceanic regions, based on the digital isochron map of the ocean floor [Müller *et al.*, 1997], the rotation models of the plates and paleoplates [Royer *et al.*, 1992], and the modeling approach of Dyment and Arkani-Hamed [1998]. Using this global remanent magnetization model together with the global VIS model, the vertical field anomaly is predicted at satellite altitude and compared with the corresponding CHAMP vertical field anomaly map. Following up on discrepancies between the predicted and the observed anomaly maps over the continents, this paper, in particular, seeks to reveal the lateral extent, magnetization level and thickness of the Precambrian provinces overlain by younger Phanerozoic crust.

2. Preparation of the Global Magnetization Model

[7] The varying pattern of Earth’s regional magnetic anomalies is caused by a superposition of geological features in the crust, covering a broad spectrum of wavelengths. These anomalies are caused by lateral variations in the magnetization of the crust. As found by Hall [1974] and Pilkington and Percival [1999], some long wavelength crustal anomalies correlate with exposed upper crustal sources. This appears to indicate that the upper crustal magnetization could be an important contributor to long wavelength anomalies, although one has to consider that lower crustal composition is often reflected in surface geology. Blakely and Griscom [1988] upward continued the aeromagnetic map of North America and found good correlations of anomalies with Precambrian and Paleozoic provinces. In another study of granitoid samples from various regions, Chappell *et al.* [1988] demonstrated that the composition of granitoids largely reflects the composition of their source regions in the lower crust. It was stressed that the distribution of granitoid suites can be used to define terranes, within each of which the lower crust has distinctive geochemical characteristics. The results from these geophysical and geochemical investigations encouraged us to derive a magnetization model based on the global distribution of geological provinces. Figure 1 shows the global distribution of geological provinces as given by the UNESCO world geological map [Commission for the Geological Map of the World (CGMW), 2000]. These geological provinces are provided as polygons in the digital version of the map used in this study.

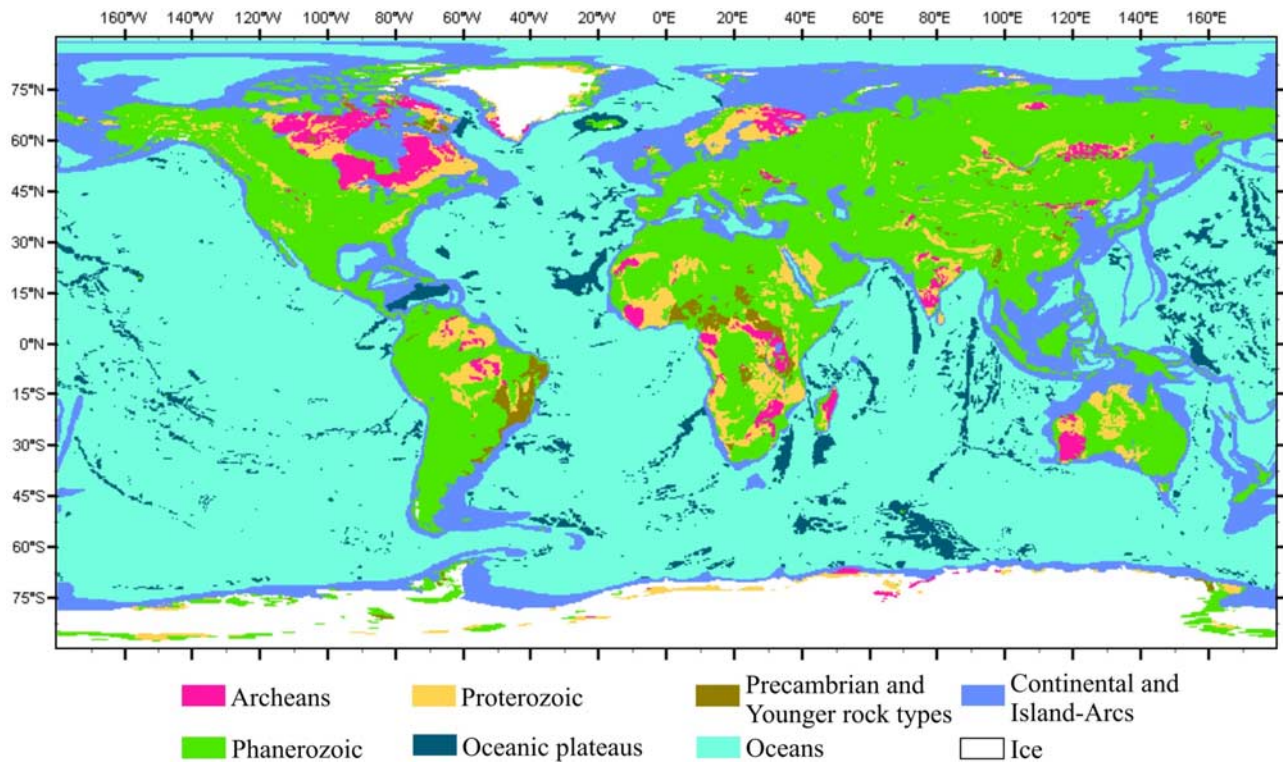


Figure 1. World geological map [CGMW, 2000] showing the distribution of the major geological provinces. Unfortunately, the largest part of the Precambrian crust is hidden by Phanerozoic. Note that only the largest polygons are drawn here.

2.1. A Geographical Information System (GIS) Approach

[8] To derive a global magnetization model, a GIS technique is developed here. A GIS is particularly convenient whenever several sets of spatially related information are to be combined [Rosenbaum and Nathanael, 1996; Pro-Ledesma, 2000]. Source information can then easily be edited, substituted or extended. The geological, petrological and seismic thickness information is represented as layers of information and these layers are combined through rules defined in the GIS system to a global magnetization model. Figure 2 shows the different layers or sets of information combined in steps to finally derive a vertically integrated susceptibility (VIS) model. The modeling starts by taking the world geological map, supplemented with tectonic maps, as a layer where the geological provinces are represented by polygons. Each of these polygons is then represented by an average susceptibility value, which is briefly explained in section 2.2. In the next step, the polygon map is converted to a grid map or a raster image of resolution $0.25^\circ \times 0.25^\circ$ (27.8×27.8 km at the Equator). Here, each grid cell inherits a susceptibility value from its parent polygon value. The seismic crustal thickness model is available as $2^\circ \times 2^\circ$ grid. The susceptibility and seismic grids are then multiplied to compute a VIS map of resolution $0.25^\circ \times 0.25^\circ$. The derivation of a VIS value for a geological region within a continent, is described in the following section. This methodology is extended for all the geological regions of the world and combined together to derive a global VIS model. In a separate step, the GIS is

also used to compute a grid of the vertically integrated remanent magnetization (VIM) from layers of ocean age and paleorotation information.

2.1.1. Continental Regions

[9] In modeling the continental crust, we draw a distinction between Precambrian units which are the major source of magnetic anomalies, and younger, usually less magnetic Phanerozoic crust. The bulk of Earth’s Precambrian crust is located in nine Precambrian cratons, which lie at the centers of the main continental masses. The Precambrian cratons

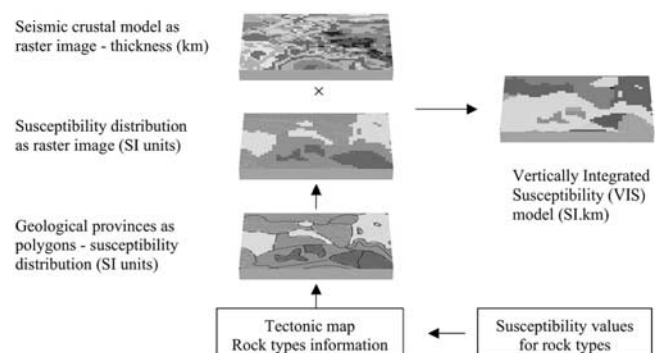


Figure 2. Flow diagram showing the different layers of information combined together on the GIS platform to compute a global vertically integrated susceptibility (VIS) model.

comprise both the exposed shields, generally termed cratons, and the buried, i.e., sub-Phanerozoic called Precambrian basement. The major cratons studied here are the Cathaysian (both China and India), Siberian, East European, Greenland, South American, North American, African, Australian and Antarctic cratons, described in detail by *Goodwin* [1991, 1996]. The derived VIS values for different geological regions within these major cratons can be found in the work of *Hemant* [2003].

[10] The younger Phanerozoic (<570 Ma) crust comprises Cenozoic, Mesozoic and Paleozoic belts. They are composed of a variety of rock types [*Condie*, 1989]. To simplify the extensive modeling process, these Phanerozoic provinces are assigned a blanket susceptibility value of 0.01 SI, which is a realistic average of typical young continental rock types. In many regions of the world, Precambrian basement underlies these provinces. Using the ferrous oxide ratio of lower/upper of 1.6 for young crust [*Taylor and McLennan*, 1985], the lower crust of the Phanerozoic provinces is assigned an average susceptibility value of 0.016 SI. However, if basement below Phanerozoic provinces is known to be of older age, then a susceptibility value appropriate for the presumed older rock types is assigned to this basement. For example, the Moscow Syncline covering most of the central East European Craton, is almost entirely underlain by 23 small to large Archean blocks with intervening Early Proterozoic fold belts [*Goodwin*, 1991]. Hence the basement below Moscow Syncline is assumed to be Archean.

2.1.2. Oceanic Regions

[11] The oceanic crust is generally divided into three layers [*Kearey and Vine*, 1990]. Layer 1, 0–1 km thick, is sediment. Layer 2, the middle layer, is made up of basalts. Layer 2 is further subdivided into an upper portion of extruded basalt, layer 2A, and a lower portion of basalt massively intruded by dikes, layer 2B. Layer 3 is gabbroic in composition. *White et al.* [1992] estimate a thickness of 2.11 ± 0.55 km for layer 2 and 4.97 ± 0.90 km for layer 3. To derive the VIS model for the oceans, the three-layered model of *White et al.* [1992] is used, of which the top sedimentary layer is considered nonmagnetic. A susceptibility value of 0.066 SI for layer 2 and 0.049 SI for layer 3 is used here. However, 10% of the oceanic floor consists of oceanic plateaus, and they show up as strong magnetic anomalies in the observed anomaly map [*Maus et al.*, 2002]. The geology of the plateaus is poorly known and there is an ongoing controversy about their origin. The present positions of scattered oceanic plateaus, especially in the southern hemisphere, are significant as they can reveal the dynamics of Gondwana breakup [*Reeves and de Wit*, 2000]. It is therefore important for us to model these features accurately, based on their proposed structure. Combining the information available from the Ocean Deep Drilling Program (ODP), seismic constraints, and the work of *Carlson et al.* [1980] and *Nur and Ben-Avraham* [1982], these oceanic plateaus are represented as a three-layered model. Layer 1 basalts and dikes; layer 2 gabbro; and layer 3 largely inferred to be either ophiolites or serpentinized ultramafic (peridotites) or olivine rich gabbro. The susceptibility values for layers 1 and 2 are taken as identical to the oceanic crust, while a high value of 0.2 SI is assigned to layer 3, assuming it to consist of ultramafic peridotites.

2.1.3. Continental and Island Arcs

[12] The remaining provinces of the world are occupied by continental and island arcs and are composed dominantly of young volcanic and plutonic rocks and derivative sediments. These regions are marked in dark blue in the world geological map [*CGMW*, 2000] and are assumed here to have the same crustal structure all across the globe (Figure 1). The upper crustal layer consists of granite and granodiorites while the lower crustal layer is dominantly of quartz diorite, a composition which is largely inferred from seismic investigations [*Condie*, 1989]. Maximum susceptibility values of 0.056 SI for the upper crust and 0.0127 SI for the lower crust (following *Hahn et al.* [1984]) are used here.

2.2. Vertically Integrated Susceptibility Model

[13] Estimating the vertically integrated susceptibility at a particular location starts with selecting the corresponding geological unit from the world geological map (Figure 1). The detailed information about rock types for the region is supplemented from the tectonic map of the region [*Goodwin*, 1991, 1996]. All the known rock types for this geological region are compiled and, using their maximum volume susceptibility value [*Clark and Emerson*, 1991; *Hunt et al.*, 1995], an average maximum susceptibility value is computed and assigned to this region. The actual susceptibility of all the rock types is assumed to be a fixed percentage of this average maximum value. An optimum value of 55% was found to minimize the root mean square difference between the Gauss coefficients of the predicted and the observed field [*Hemant*, 2003]. This scaling factor of 0.55 for the average maximum susceptibility is used as a global constant for all rock types. Next, the stratigraphical thickness, known from drilling or seismic investigations, for each geological stratum within the vertical column is multiplied by the average susceptibility of that stratum. Figure 3 shows a typical geological cross section for which a VIS value is computed. The symbols in Figure 3 represent h the thickness, χ the average susceptibility of the stratum, and (θ, λ) the latitude and longitude of the geological province on the world map. As an example, the method is applied to derive the maximum susceptibility value for the Ashuanipi Complex in the eastern Superior Province in the North American Craton. The rock types exposed and their maximum susceptibility values in the Ashuanipi Complex [*Goodwin*, 1991] are reproduced in Table 1.

[14] For regions devoid of any stratigraphical information, for e.g., Ashuanipi Complex, the average susceptibilities are multiplied with the crustal thickness of the upper crust known from the global seismic models like 3SMAC [*Nataf and Ricard*, 1996] and CRUST2.0 [*Bassin et al.*, 2000]. The susceptibility value for the lower crust in any geologic region is computed by multiplying the average susceptibility of the upper crust with a factor accounting for the difference in the iron oxide content in the average composition of the upper and the lower crust [*Taylor and McLennan*, 1985]. This gives a factor of 1.2 for the Archean and 1.6 for the post-Archean provinces. One of the important assumptions in the present work is to consider the seismic Moho as a magnetic boundary [*Wasilewski and Mayhew*, 1992]. Thus the upper mantle is

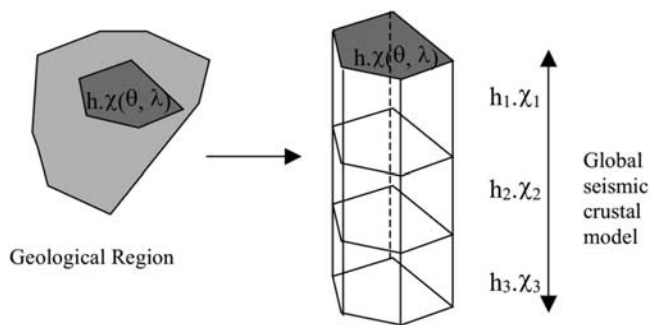


Figure 3. Sample geological cross section of a region for which a VIS value is computed. The symbols are explained in the text.

assumed to be nonmagnetic. Then the VIS value for the Ashuanipi Complex can be computed as follows:

$$\text{VIS} = 0.55 * \text{xashnp} * (\text{sm3u} + 1.2 * \text{sm3l})$$

where sm3u is thickness of the upper crust from the CRUST2.0 model, sm3l is thickness of the lower crust from the CRUST2.0 model, and the factors 0.55 and 1.2 are explained in the text above.

[15] Each geological province is modeled following the above steps to compute the VIS value for that province. Finally, VIS values for all geological provinces (continents, oceans, and continental and island arcs) are combined to derive a global VIS model which is shown in Figure 4.

2.3. Contribution of Remanent Magnetization

2.3.1. Continental and Oceanic Crust

[16] Within the continental crust, stable remanence is likely to be less important in deep crustal conditions than in upper crustal conditions [Shive *et al.*, 1992]. Stable remanence decreases with increasing temperature and degree of metamorphism and is therefore unlikely to be responsible for the strong magnetization required to explain the continental magnetic anomalies. Treloar *et al.* [1986] showed through laboratory and theoretical studies that even viscous remanent magnetization in the lower crust is unlikely to be as strong as induced magnetization. Moreover, the size of iron(Fe)-titanium(Ti) oxides are estimated to be around 100 microns in the lower crust [Schlinger, 1985], i.e., they are not single-domain grained minerals, and hence cannot carry strong remanence. Single-domain grain bearing rocks like basalts are the most effective carrier of stable remanence. Shive [1989] and Shive *et al.* [1992] therefore concluded that the total magnetization of lower crustal rocks is not significantly greater than their induced magnetization. However, this line of reasoning is contradicted, by a recent experimental study of naturally exsolved hematite-ilmenite samples under mid-to-lower crustal temperature and pressure conditions, where it was shown that in areas of a cool cratonic crust, these samples retain a high remanent component, and, in warmer regions, coarsened hematite lamella effectively retain a remanent component with a relatively high coercivity [McEnroe *et al.*, 2004]. The study showed that natural samples have average natural remanent magnet-

izations (NRMs) of 25 A/m, of which 95% of the NRM retained to 600°C. The thermal stability was high and above that of magnetite. The samples had an average ratio of remanent to induced magnetization of $Q = 47$, clearly indicating a possibly significant role of remanence. This is supported by Magsat anomaly studies which find indications for remanence in the lower continental crust of Europe [Taylor and Ravat, 1995; Pucher and Wonik, 1998]. However, since every magnetic anomaly can be explained by induced magnetization, induced and remanent magnetization cannot be distinguished from the magnetic anomalies alone.

[17] Unfortunately, drill cores from the Continental Deep Drilling Program, KTB [Berckhemer *et al.*, 1997], are, in general, not suitable for paleomagnetic investigations, due to unstable natural remanent magnetization (NRM) and often have a drilling-induced remanence overprint [Pohl *et al.*, 1991; Worm and Rolf, 1994]. Moreover, global data of remanent magnetization for the continental crust is largely incomplete and, for these reasons, remanence is not considered for the continents in the preparation of our global magnetization model.

[18] The situation is different over the oceans, where the magnetic strips of alternate polarization, parallel to the mid-oceanic ridges, are seen prominently in aeromagnetic and shipborne magnetic maps [Verhoef *et al.*, 1996]. However, these are mostly absent at satellite altitude (Figure 5) because the fields from the alternating remanent magnetization of the spreading oceanic crust tend to cancel at satellite altitude [LaBrecque and Raymond, 1985]. There are, however, other strong anomaly features parallel to the mid-oceanic ridges, prominent over the North Atlantic Ocean and off the coast of Indian peninsula. These Cretaceous Quiet Zones acquired their remanent magnetization during the Cretaceous Long Normal (CLN) polarity interval. We use the methods of LaBrecque and Raymond [1985] and Purucker and Dymant [2000] to build a remanent magnetization model for the oceanic crust. Remanence of the oceanic crust arises due to a combination of primary and secondary magnetization. The primary magnetization is acquired as the oceanic crust forming at the mid-oceanic ridges cools to below the Curie temperature of the magnetic minerals. This magnetization is a thermoremanent magnetization (TRM) and the direction of this acquired magnetization is along the geomagnetic main

Table 1. Rock Types Exposed at the Ashuanipi Complex, Superior Province and Their Maximum Susceptibility Values^a

Rock Types	Maximum Susceptibility Value
Migmatites	0.025
Orthopyroxene	0.0018
Mafic gneiss	0.025
Tonalite	0.062
Orthogneiss	0.025
Paragneiss	0.025
Tonalite	0.062
Granite	0.05
Syenite	0.051
Pegmatite	0.082

^aThe computed maximum susceptibility value for the complex is average maximum susceptibility value (xashnp) of $(0.025 + 0.0018 + 0.025 + 0.062 + 0.025 + 0.025 + 0.062 + 0.05 + 0.051 + 0.082)/10 = 0.041$ SI.

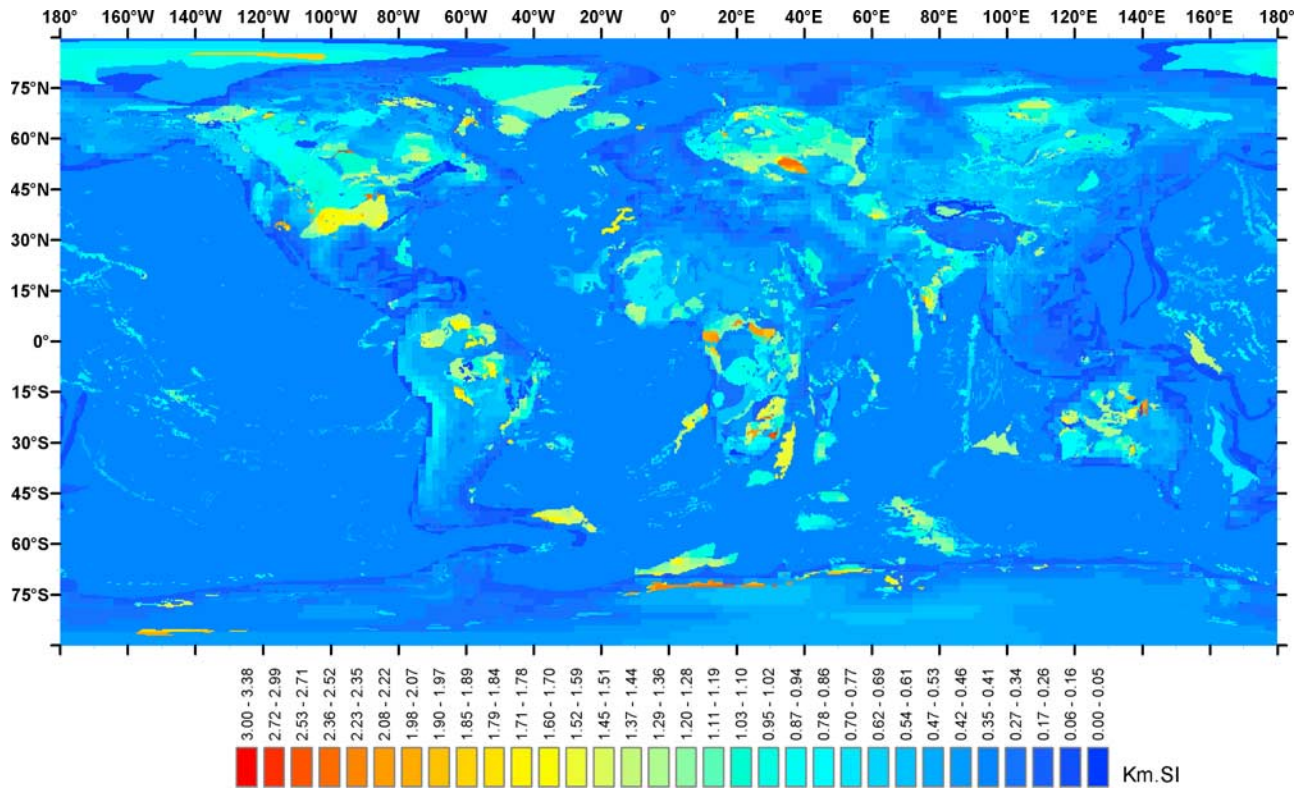


Figure 4. VIS map of the world.

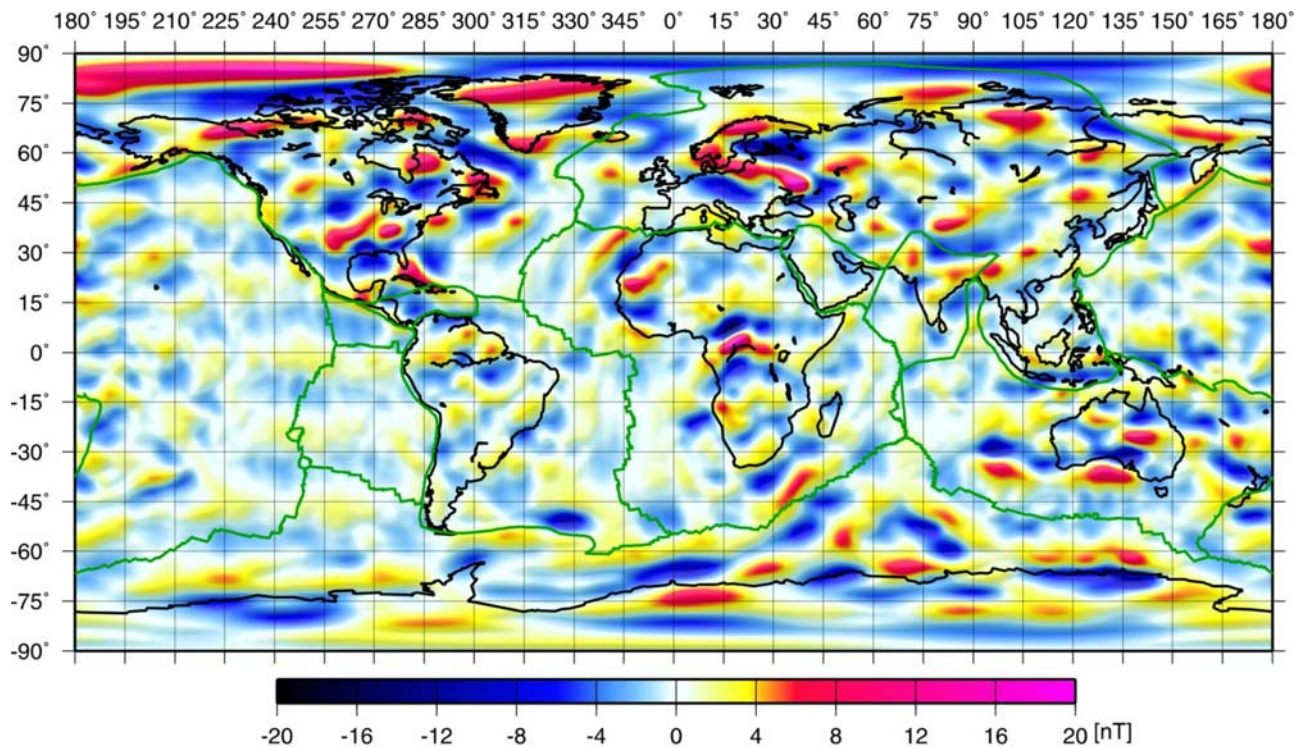


Figure 5. Observed vertical field anomaly map for spherical harmonic degrees 16–90 at an altitude of 400 km, as given by the MF3 model derived from CHAMP satellite magnetic measurements (<http://www.gfz-potsdam.de/pb2/pb23/SatMag/litmod3.html>).

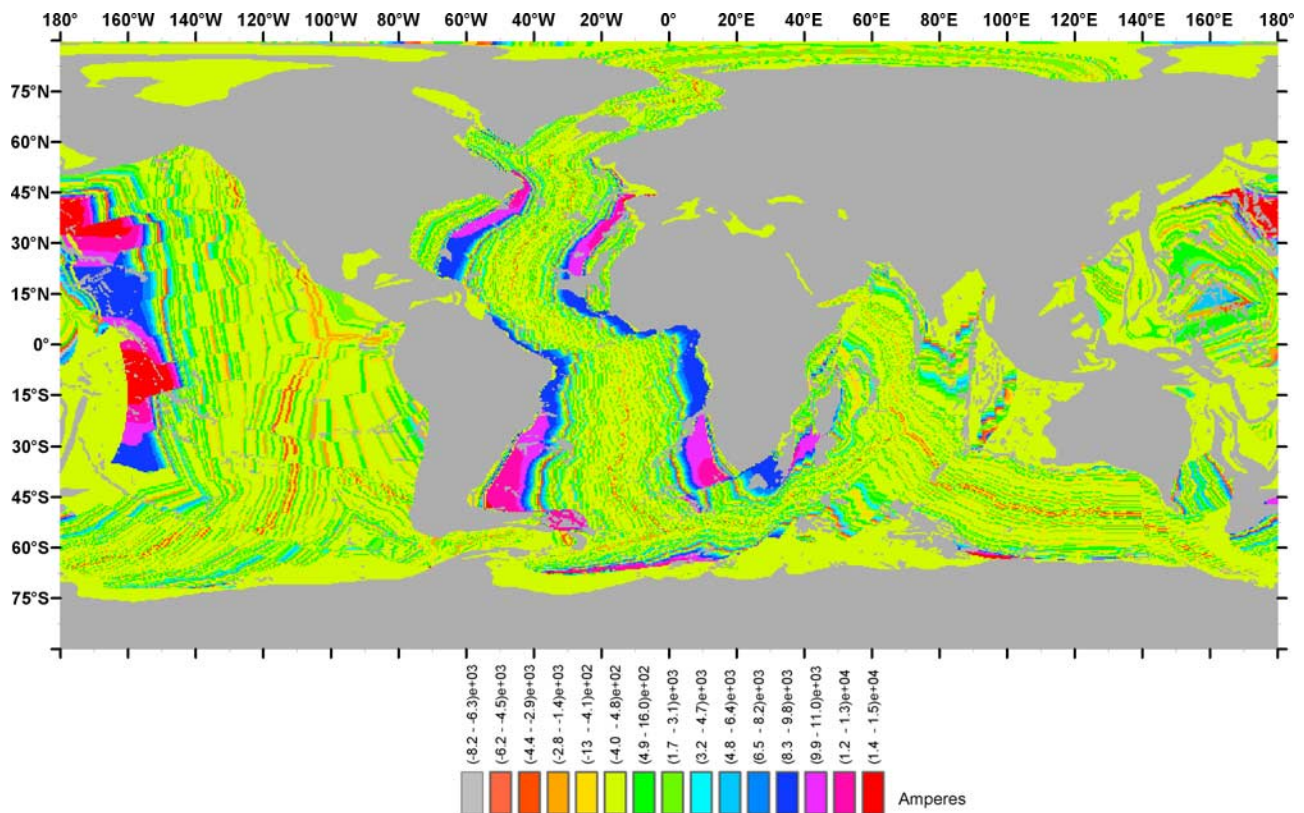


Figure 6. Vertically integrated remanent magnetization (VIM) in oceanic regions. Grey patches overlain on oceanic isochrons are oceanic plateaus.

field of the geological age during which the crust was formed [Butler, 1992]. The secondary magnetization, or chemical remanent magnetization (CRM), is acquired as a result of chemical changes of the original oceanic crust as it cools. The CRM points in the direction of the geomagnetic main field at the time of chemical alteration, which is retarded by several million years from the time of formation of the oceanic crust [Dyment and Arkani-Hamed, 1998].

2.3.2. Derivation of Vertically Integrated Magnetization (VIM) Model

[19] The anomaly pattern over the oceans is largely due to the intensity and the direction of the remanent magnetization of each isochron in the oceanic floor. We follow the procedures discussed by Dyment and Arkani-Hamed [1998] to compute the intensity and the vector directions of all isochrons. Following Raymond and LaBrecque [1987], the CRM is modeled to grow exponentially in time, while directly related to the exponential decay of the TRM. The sum of these processes results in a net magnetization value that reflects the total acquired magnetization during any geological period. The acquired magnetization is a function of two parameters, the decay constant λ and the ratio of CRM to TRM. Following Raymond and LaBrecque [1987], the decay constant λ was assigned a value 5.0 Ma and the CRM:TRM ratio was chosen to be 4:1. The parameters of the input crustal model discussed above differ from the three input models discussed by Dyment and Arkani-Hamed [1998]. We do not consider the magnetization to extend below the oceanic Moho in contrast to the assumptions of

Dyment and Arkani-Hamed [1998]. Our crustal model is composed of 3 layers (top to bottom): Layer 2A, extrusive basalts having a thickness of 0.5 km and NRM of 4.0 A/m, layer 2B, intrusive basalts of thickness 1.61 km and NRM 0.0 A/m and layer 3, Gabbro of thickness 4.97 km and NRM 0.25 A/m. Using the digital isochron map of the oceanic crust [Müller et al., 1997] and decay model of TRM and CRM superimposed on the polarity of the isochrons [Gradstein et al., 1994; Cande and Kent, 1995], and following procedures outlined by Dyment and Arkani-Hamed [1998], the VIM map of the oceanic crust (Figure 6) is computed by multiplying the saturation magnetization with the thickness of the crust. The spatial variation of the paleodipole field intensity ($s = \sqrt{1 + 3 \cos^2 \theta}$, where θ is the geographic colatitude and the average paleofield is assumed to be dipolar and aligned with the Earth's spin axis) is also taken into account. The VIM value for oceanic regions of unknown age is set to zero. This introduces fictitious anomalies over the edges or near the boundaries, where oceanic crust of known age borders with crust of unknown age. However, these spurious anomalies are very small in amplitude at satellite altitude.

[20] The directions or the unit vectors of the remanent magnetization for each isochron are computed using rotation models of Royer et al. [1992], combined with the apparent polar wander (APW) path for Africa [Ziegler et al., 1983], following the work of Dyment and Arkani-Hamed [1998]. For this, the paleoposition of each isochron is computed. It is assumed that the paleomagnetic field was dipolar and that geomagnetic and geographic poles coincide

during a geological time period. Following *Cox and Hart* [1986], the original coordinates of each isochron were computed from its present-day geographic position. The paleoinclination at each point on the isochron can be computed using the respective paleoposition information, following

$$\tan \Theta = \tan I/2$$

where Θ is the paleolatitude and I is the paleoinclination. The paleodeclination of the remanent magnetization is computed by applying the finite rotation forward in time [*Dyment and Arkani-Hamed*, 1998]. Unit vectors of remanent magnetization were computed using these derived paleoinclination and paleodeclinations.

2.4. Curie Isotherm

[21] Our global magnetization model does not incorporate Curie temperature-depth (CTD) variation within the crust. The reason is that the global distribution of the temperature-depth variation is still not available in the required spatial resolution and accuracy [*Artemieva and Mooney*, 2001]. *Frost and Shive* [1986], based on the measured geothermal gradients, computed the 600°C isotherm and concluded that it is within the lower crust at depths of around 20 km in areas like the Basin and Range province. Below cratons and shields, on the other hand, the isotherm could be below the Moho. However, *Wasilewski and Mayhew* [1992] found a complete absence of magnetite in mantle peridotites, except in few pockets of serpentinized upper mantle [*Haggerty*, 1978]. They therefore concluded that the Moho is the lower magnetic boundary. Over the oceans, the serpentinized upper mantle, as argued by *Arkani-Hamed and Strangway* [1986] could add to anomalies observed at satellite altitude. However, their studies were restricted to subduction zones. In summary, we expect that the Curie isotherm is above the Moho in hot regions, while it is identical to the Moho in cold regions. Arguably the most accurate geothermal model, by *Artemieva and Mooney* [2001], has a spatial resolution of only $10^\circ \times 10^\circ$, which is too coarse for the present study. Thus we did not incorporate a temperature model, relying on the more accurately known Moho as a lower magnetic boundary, instead.

3. Prediction of the Crustal Magnetic Field at Satellite Altitude

[22] An equivalent dipole method is used to compute the magnetic potential. The method works in two phases. First, the magnetic potential due to induced magnetization is computed with the VIS model as input. Next, the potential is computed for remanent magnetization with the intensity and the unit vectors of the VIM model as input. To compute the magnetic potential of the field due to induced magnetization, the VIS model is replaced with a distribution of equivalent dipoles at the surface, representing an induced magnetization in the direction of the main field \mathbf{B} of the Earth. Consider a volume element $d\tau'$ of magnetizable material within the Earth's crust, located at point $\mathbf{r}' = (r', \theta', \phi')$, with radius r' , colatitude θ' and longitude ϕ' . Note that r' is adjusted for the ellipticity of the Earth thus has a smaller value at the poles than at the equator. This magne-

tized volume element $d\tau'$ contributes to the potential V at a fixed external point $\mathbf{r} = (r, \theta, \phi)$ by dV , given as

$$dV(\mathbf{r}, \mathbf{r}') = \frac{\mu_0}{4\pi} \mathbf{dm}(\mathbf{r}') \cdot \frac{\mathbf{R}}{|\mathbf{R}|^3}, \quad (1)$$

where μ_0 is the permeability of free space, $R = |\mathbf{r} - \mathbf{r}'|$, and $\mathbf{dm}(\mathbf{r}')$ is the dipole moment and is the product of $d\tau'$ with the magnetization \mathbf{M} . Since the crustal thickness d is negligible compared to the satellite altitude, the crustal magnetization can be modeled as a thin ellipsoidal sheet, with the integrated susceptibility of the crust defined as

$$\tilde{\chi}(\theta', \phi') = \int \chi(r', \theta', \phi') dr' \quad (2)$$

where the vertical integration is over the thickness of the Earth's crust and $\tilde{\chi}(\theta', \phi')$ is the vertically integrated magnetic susceptibility in a thin sheet on the ellipsoidal Earth surface. The dipole moment $\mathbf{dm}(\mathbf{r}')$ is then related to $\tilde{\chi}(\theta', \phi')$ by

$$\mathbf{dm}(\mathbf{r}') = \mathbf{dm}(r', \theta', \phi') = \tilde{\mathbf{M}}(\theta', \phi') ds' = \frac{1}{\mu_0} \tilde{\chi}(\theta', \phi') \mathbf{B}(\mathbf{r}') ds' \quad (3)$$

where $\tilde{\mathbf{M}}$ is the vertically integrated magnetization and ds' is a surface element. Inserting equation (3) into (1) gives

$$dV(\mathbf{r}, \mathbf{r}') = \frac{1}{4\pi} \tilde{\chi}(\theta', \phi') \frac{\mathbf{B}(\mathbf{r}') \cdot \mathbf{R}}{|\mathbf{R}|^3} ds' \quad (4)$$

In the thin shell approximation, the volume element $d\tau'$ degenerates to the area ds' . To efficiently compute the spherical harmonic coefficients of the potential, the potential V is calculated at the Gauss-Legendre points on an irregular spherical grid at an altitude of 400 km above the mean Earth radius, by summing the contribution of each crustal source dipole.

[23] To compute the potential of the field due to remanent magnetization, the inputs are the intensity and the unit vectors of the VIM model or bulk remanent magnetization. For this, equation (4) is adapted in such a way that the integrated susceptibility $\tilde{\chi}(\theta', \phi')$ is replaced by $\mu_0 \cdot I_0$, where I_0 is the intensity of bulk remanent magnetization. The second element $\mathbf{B}(\mathbf{r}') \cdot \mathbf{R}$ is replaced by $\boldsymbol{\nu} \cdot \mathbf{R}$, where $\boldsymbol{\nu}$ is a unit vector in the direction of bulk remanent magnetization. The contribution dV_m to the magnetic potential for remanent magnetization, then reads as

$$dV_m(\mathbf{r}, \mathbf{r}') = \frac{1}{4\pi} \mu_0 \cdot I_0 \frac{\boldsymbol{\nu} \cdot \mathbf{R}}{|\mathbf{R}|^3} ds' \quad (5)$$

[24] The Gauss coefficients of the potential of the remanent magnetic field are computed following the same procedure as outlined above for the induced magnetization. The spherical harmonic expansion of the potential can be written in the usual way [*Blakely*, 1995] as

$$V(r, \theta, \phi) = a \sum_{n=1}^n \sum_{m=0}^n \left(\frac{a}{r}\right)^{n+1} (g_n^m \cos m\phi + h_n^m \sin m\phi) P_n^m(\cos \theta) \quad (6)$$

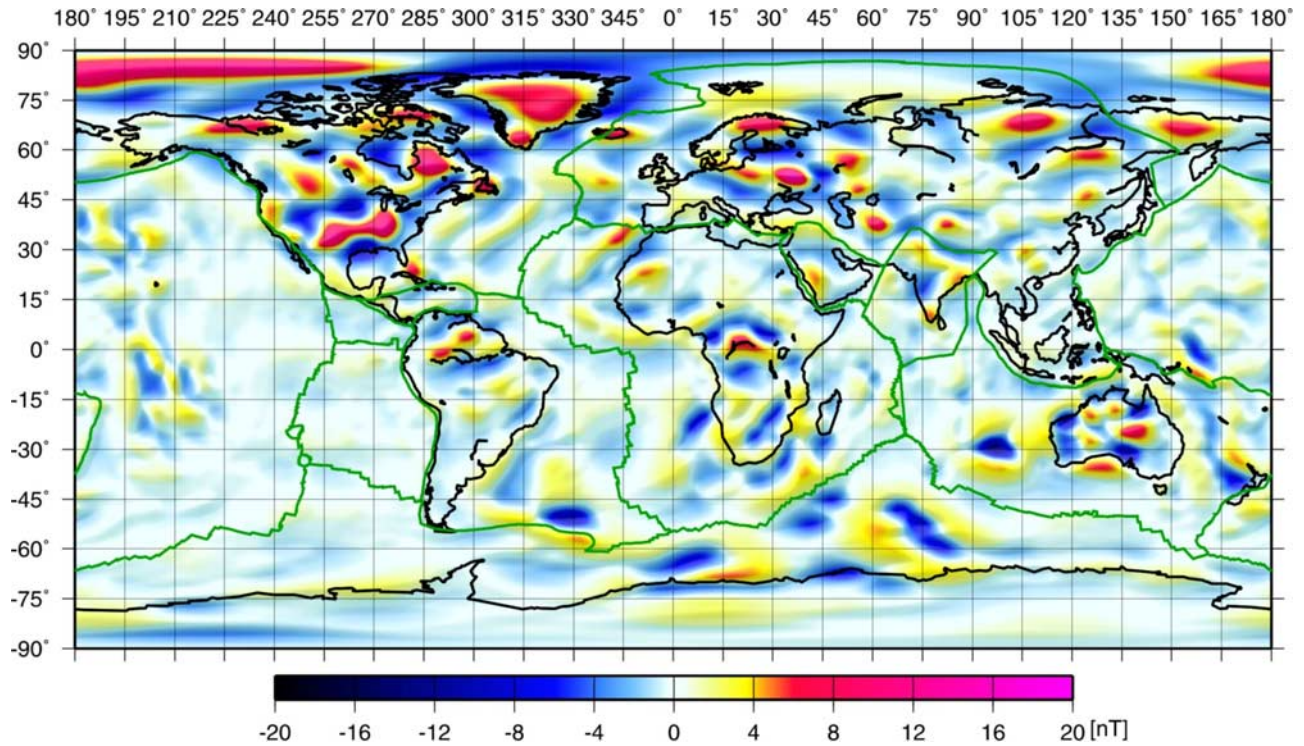


Figure 7. Predicted vertical field anomaly map (initial model) for spherical harmonic degrees 16–90 at an altitude of 400 km.

with the magnetic reference radius $a = 6371.2$ km, Gauss coefficients g_n^m and h_n^m , degree n and order m , and P_n^m are the associated Legendre functions. The Gauss coefficients obtained for induced and remanent magnetizations are then added to obtain the combined Gauss coefficients of the potential of the predicted magnetic anomaly.

[25] The predicted crustal magnetic field \mathbf{B} is related to its potential by

$$\mathbf{B}(r, \theta, \phi) = -\nabla V(r, \theta, \phi) \quad (7)$$

Using equation (7), the three vector components $B_r(r, \theta, \phi)$, $B_\theta(r, \theta, \phi)$, and $B_\phi(r, \theta, \phi)$ of the crustal magnetic field can be computed in spherical coordinates. The z component of the crustal magnetic field is then related to the radial component and the potential of the crustal magnetic field as

$$B_z(r, \theta, \phi) = -B_r(r, \theta, \phi) = \frac{\partial V}{\partial r} = - \sum_{n=1}^n \sum_{m=0}^n (n+1) \left(\frac{a}{r}\right)^{n+2} \cdot (g_n^m \cos m\phi + h_n^m \sin m\phi) P_n^m(\cos \theta) \quad (8)$$

We choose to interpret maps of the vertical component. Unlike the scalar anomaly, the vertical component on a spherical shell completely determines the magnetic potential of the field. The predicted vertical field anomaly map is computed here using the combined Gauss coefficients of the fields of the VIS and VIM models. Spherical harmonic degrees 1–15 are set to zero because this long wavelength crustal field is masked by the main field and is not observable. Finally, only spherical harmonic degrees 16–90 of the model field are compared with the corresponding degrees 16–90 of the observed crustal field. A detailed

comparison of the predicted anomalies from our “initial model” with the observed anomalies over the continents and oceans is given in the next section. On the basis of the discrepancies of the two maps, the initial magnetization model is adapted to the observations in selected regions. The resulting improved model is called our “first iteration” model.

4. Predicted Anomaly Map and Its Initial Interpretation

[26] The vertical field anomaly map predicted at a satellite altitude of 400 km for spherical harmonic degrees 16–90 is shown in Figure 7. The predicted and observed fields are independent, except for the global scaling factor of 0.55, which adjusts the overall amplitude of the prediction to the observed field. On visual comparison with the observed CHAMP anomaly map (Figure 5) it is apparent that there are anomalies over the continental regions, where the predicted and observed maps match well. However certain discrepancies are also evident. For example, the weak east-west trending anomaly patterns over the oceanic region so prominent in the observed map, especially over the Pacific Ocean, are completely absent in the predicted map. Short wavelength contributions from the main field (SH degrees 16–20) dominate here over the weak crustal field [Dyment and Arkani-Hamed, 1998]. The predicted anomaly patterns related to oceanic rises and plateaus agree well with observations, especially those located southeast of the African continent, while only partial agreement is found in the regions southwest of Africa.

[27] Since continental crust is thicker than oceanic crust, an anomaly may have been expected over the continent-

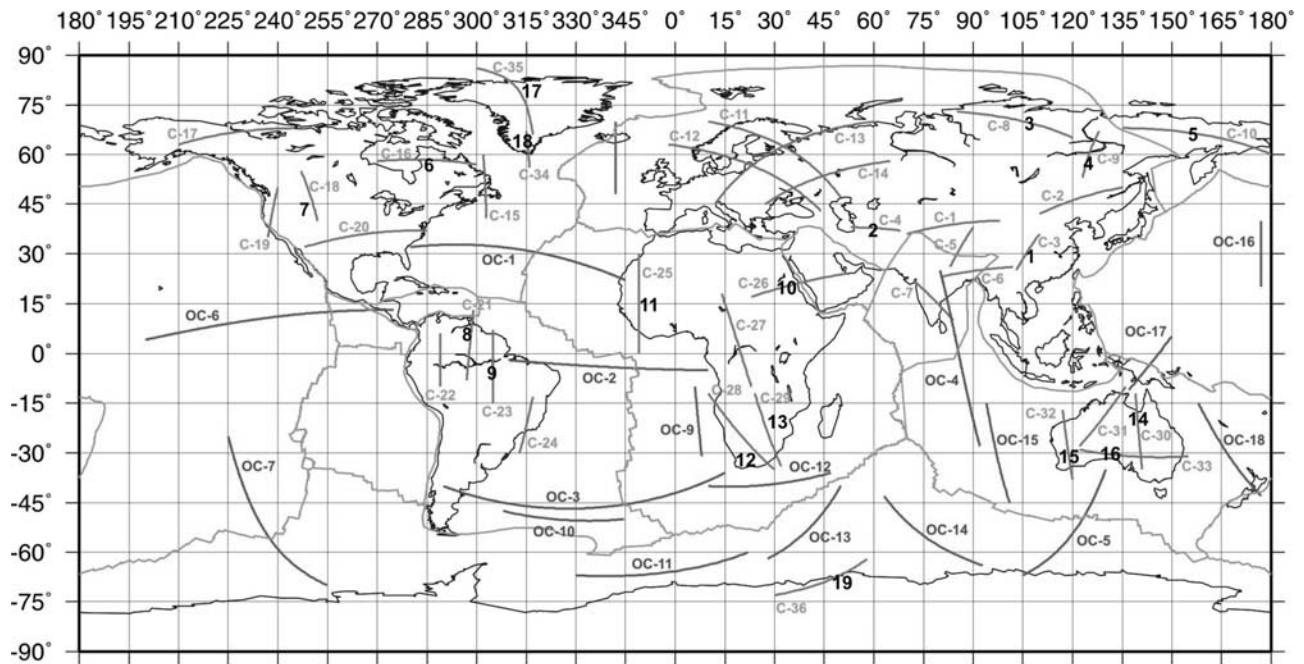


Figure 8. World map showing the profile sections and the major geological features marked by numbers over the continents and oceans. The geological feature and the profile numbers are discussed in the text.

ocean (C-O) boundary in a global crustal magnetic anomaly map. However, this anomaly is not seen over most of the C-O boundary. On the basis of the same GIS modeling technique, *Hemant and Maus* [2005] showed that an anomaly is indeed not expected over the C-O boundaries where the oceanic crust is flanked by continental regions Phanerozoic in age, while the anomaly is predicted over the boundaries where the flanking geological provinces are Precambrian in age. The study showed that the absence of a global C-O anomaly is due to the comparable VIS values for the continents and oceans on large sections of the C-O boundary.

4.1. Role of the Seismic Model Used for Crustal Thickness

[28] We were surprised to find that differences between global seismic models are large enough to be visible in the predicted crustal magnetic field. Both the 3SMAC and CRUST2.0 crustal models were used here to compute the VIS model. The predicted vertical field anomaly maps produced using these VIS models did not differ much over the oceans. However, over the continents some observed anomaly patterns were better explained by one model than the other. Significant disagreement in the predictions using the two different seismic crustal models was seen over Africa, Greenland, northern Siberia, eastern Tibetan Plateau, South America and the eastern region of the North American Craton. Except over the North American Craton, where the magnetic anomaly map produced using the CRUST2.0 matched more closely with the observed anomaly map, the 3SMAC model produced a better agreement with the observed map. Following this visual comparison, the CRUST2.0 model was used for computing the VIS model for the North American Craton, while the 3SMAC model was used for the rest of the world, except for Greenland and for Guyana Shield, South America, where the new seismic

models of *Dahl-Jensen et al.* [2003] and *Schmitz et al.* [2002] were used. For the oceans, the crustal thickness model of *White et al.* [1992] was used.

4.2. Major Anomalies Over the Continents

[29] A selected set of profiles over major geological provinces is used to compare the initial model's prediction with the observed magnetic anomalies (Figures 8, 9, 10, and 11). Profile sections C-1 to C-36 are shown for the continents in Figures 9 and 10, while Figure 11 shows profile sections OC-1 to OC-18 for the oceanic regions. The numbers referenced in parentheses discussed below correspond to geological provinces marked in Figure 8. Major anomaly features over the Precambrian provinces have largely been reproduced in the predicted anomaly map. The shapes of the predicted anomalies agree well with those of observed anomalies over the Sichuan massif (1), the Turkmenistan Shield (2) and over the northern Indian shield of the Cathaysian-Indian craton. Over the Siberian Craton, the strong anomaly predicted over the Anabar Shield (3), the Aldan Shield (4) and over the western Kolyma-Omolon Block (5) agrees with the observations. The magnetic anomalies over the Ungava Craton (6), Wyoming province (7), accreted arc terrains over the western United States in the North American Craton agree both in the predicted and the observed map. Regions of the Guyana Shield (8) and the north Brazilian shield (9) of South American craton show moderate anomaly features, which are in agreement with the predicted anomaly. Major anomaly features predicted over the Nubian Shield (10) in the east, over the Taudeni Basin (11) in the west and over the Namaqua-Natal (12) and Limpopo Belt (13) in the south, of the African craton are in agreement with the observed anomaly. The observed anomaly features over the Mount Isa Inlier (14) in the north, central and eastern Australian regions

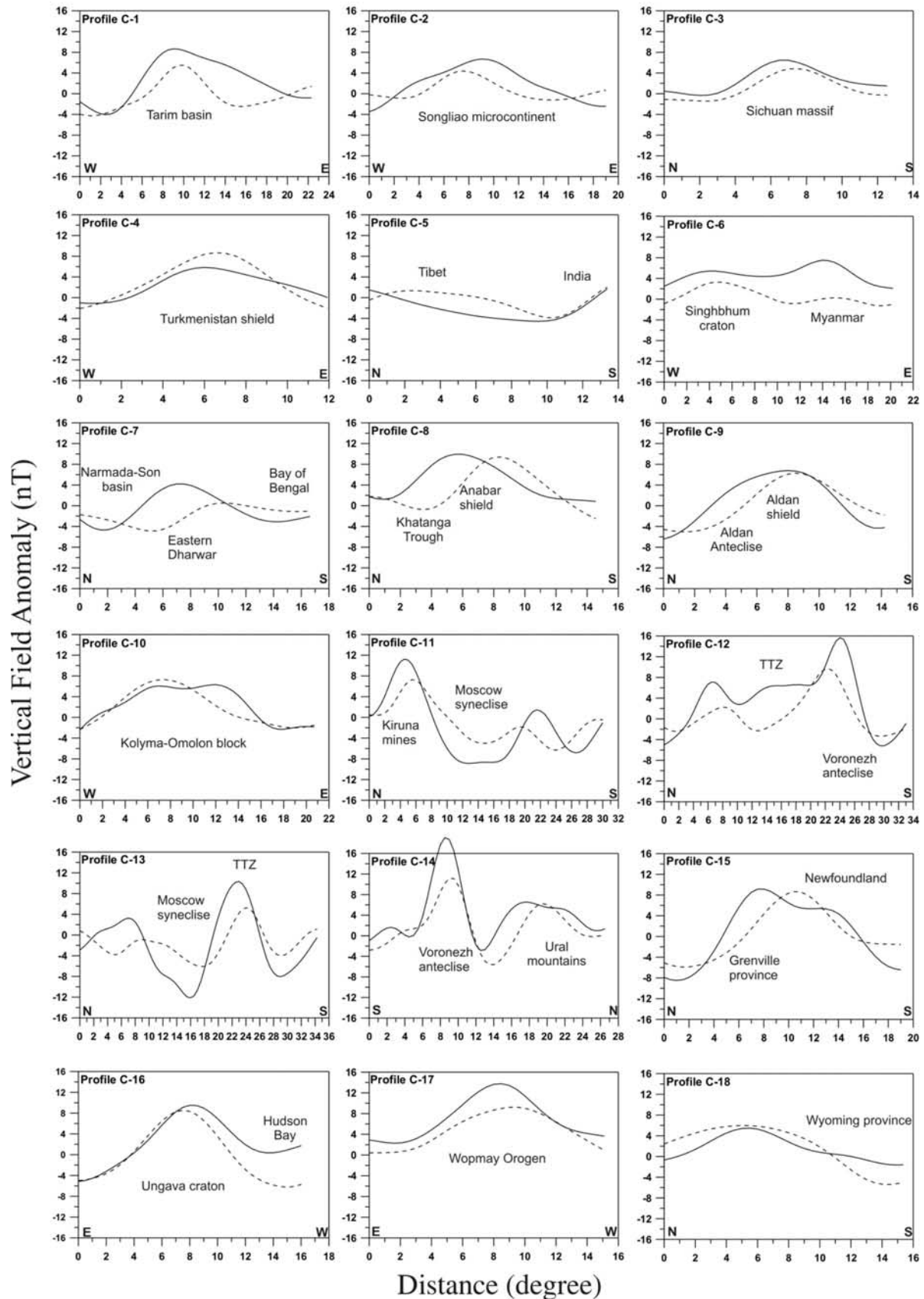


Figure 9. Profile sections (C-1 to C-18) over the continents. The profile numbers are marked in Figure 8. The solid line represents the observed value, and the dashed line represents the predicted value.

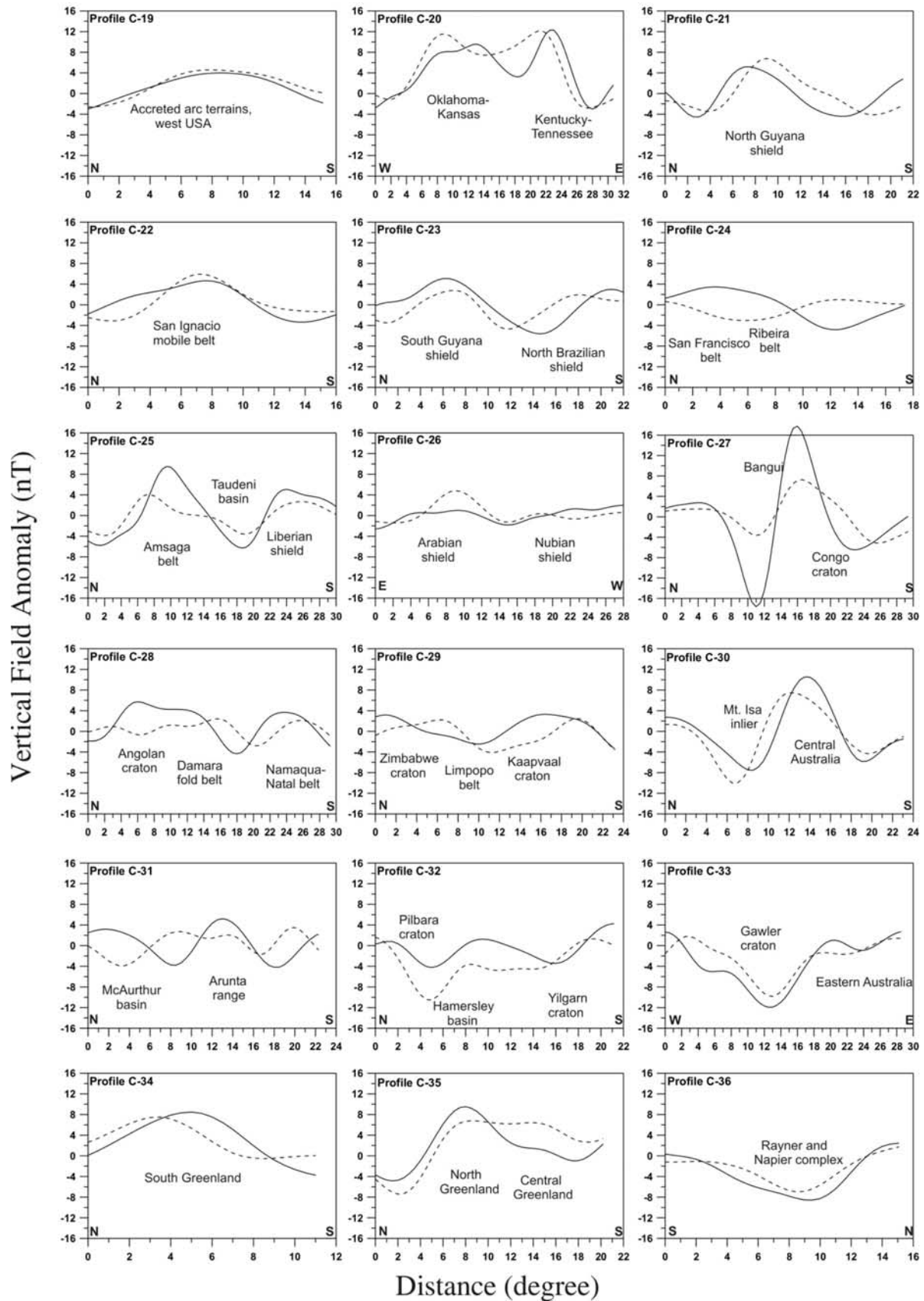


Figure 10. Profile sections (C-19 to C-36) over the continents. The profile numbers are marked in Figure 8. The solid line represents the observed value, and the dashed line represents the predicted value.

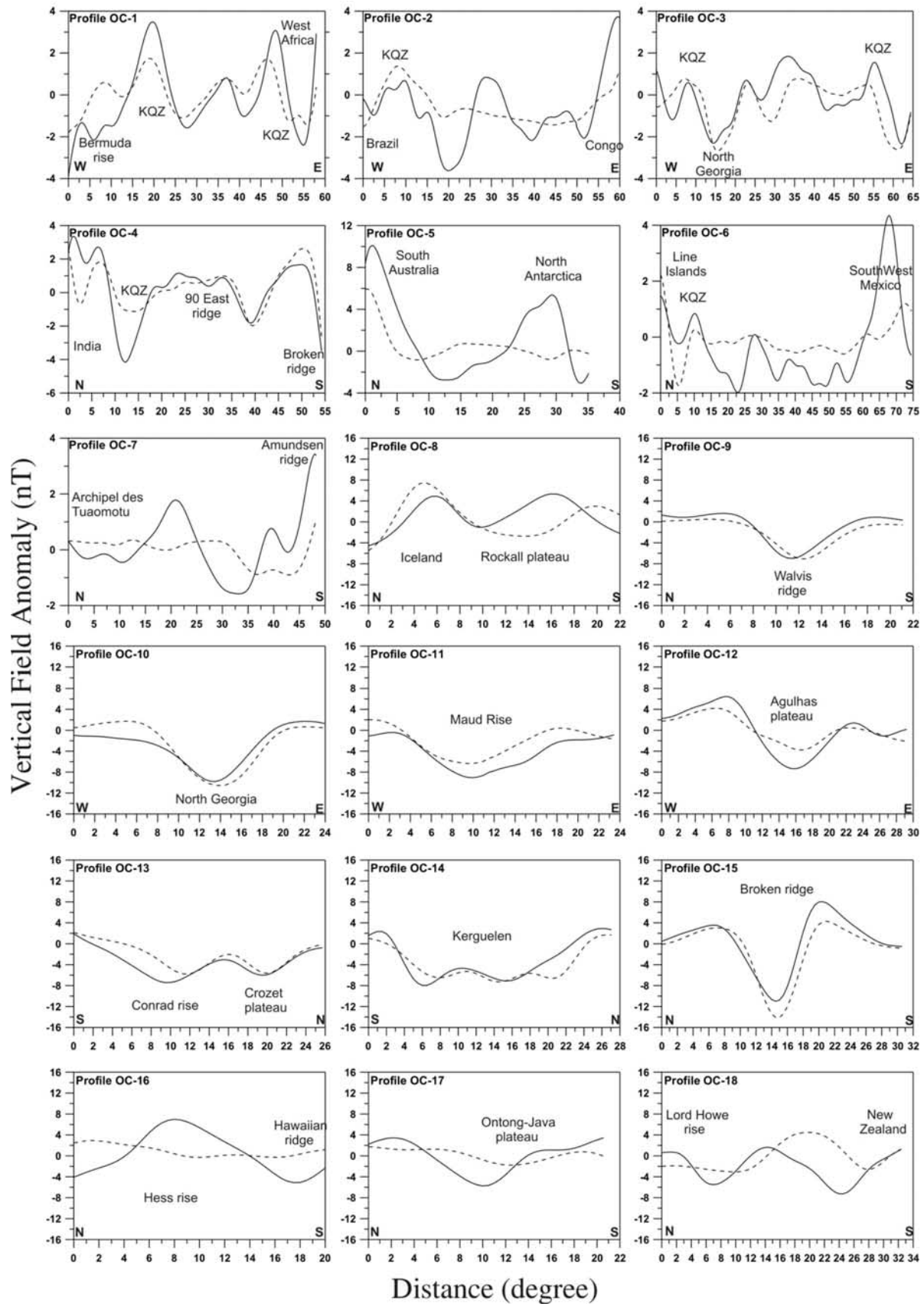


Figure 11. Profile sections (OC-1 to OC-18) over the oceanic regions. The profile numbers are marked in Figure 8. The solid line represents the observed value, and the dashed line represents the predicted value.

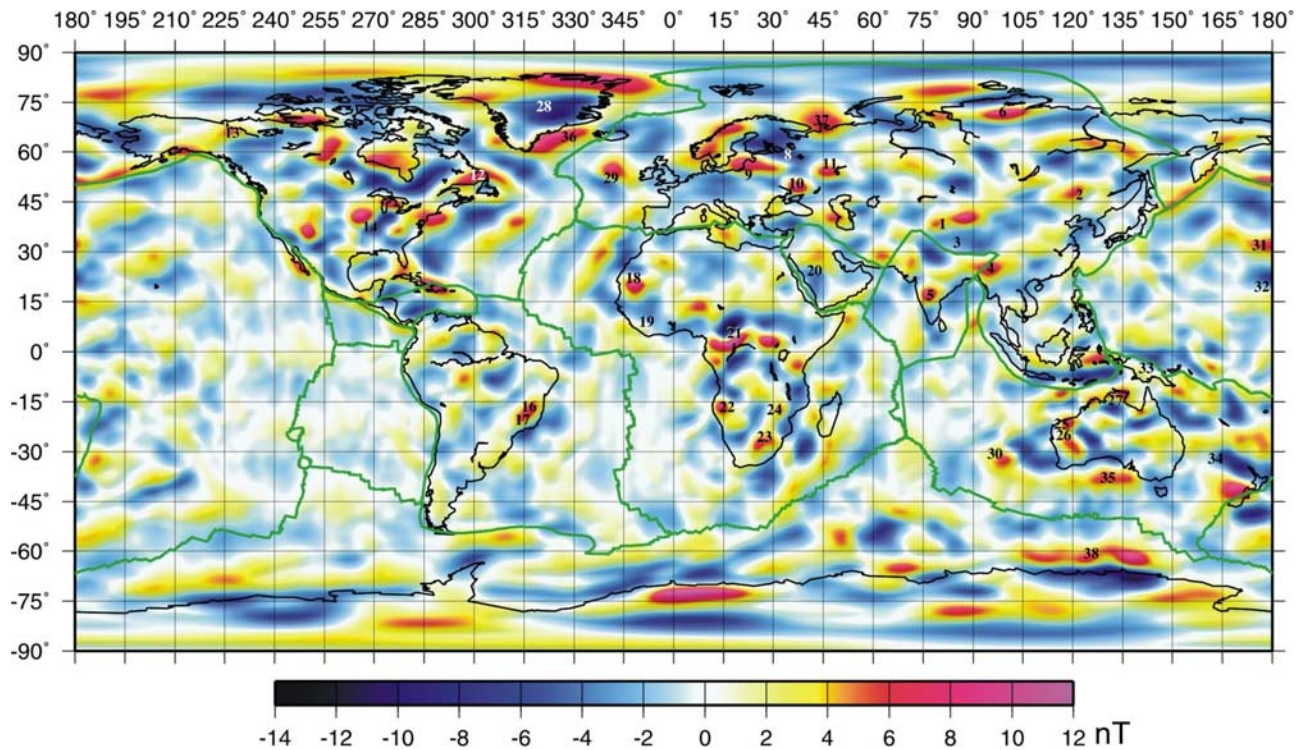


Figure 12. Vertical field magnetic anomaly map showing the difference in Figures 5 and 7. The numbers are explained in the text. Note that they indicate different locations than the ones in Figure 8.

and over the Yilgarn (15) and Gawler Craton (16) are reproduced well in the predicted anomaly map. The anomalies predicted over the northern (17) and the southern region of Greenland (18) agree with the observations. Over the well-known Rayner and Napier complexes (19) of the Antarctica, the predicted anomalies agree with observations. Over the oceans, the profiles OC-1 and OC-3 over the North and South Atlantic oceans and in the profile OC-4 over the Indian Ocean (Figure 11) demonstrate that indeed both induced and remanent magnetizations are required to explain the observed anomalies. The anomalies predicted over the major oceanic plateaus and rises in the South Atlantic and Indian oceans largely agree with the observed anomaly features.

[30] Apart from the areas of good fit to the data, partial to significant disagreements between the observed and predicted maps remains. The difference map computed by taking the difference in anomaly value between Figures 5 and 7 is shown in Figure 12. The anomaly differences lie between -4 to $+6$ nT over most of the continental and oceanic regions, but some anomaly differences exceed ± 10 nT. We have attempted to classify the most prominent discrepancies and attributed them to their most likely causes. The results are summarized in Table 2. Note that the numbers in Table 2 correspond to the numbers in Figure 12, which are different from the ones in Figure 8.

[31] The difference map (Figure 12) shows additional prominent anomaly features, along northwestern continental and coastal regions of Greenland, between Iceland and Greenland (36), east of Kola peninsula (37), Europe, an anomaly feature (38), that appears elongated due to Cylindrical equidistant map projection, between 120° and 150° E and along 62° S latitude and over parts of Antarctica. These anomaly features have not been modeled. The

numbers mentioned above in parenthesis are shown in Figure 12. There are several other small to large-scale features in Figure 12, whose causative sources have yet to be determined.

4.3. Improvement of the Initial Model and Its Geological Implications

[32] The overall agreement in the predicted and the observed magnetic anomaly maps indicates that the sources to the magnetic anomalies are indeed geological in origin and lie in the Earth's crust. However, the discrepancies between the predicted and the observed anomalies over certain regions of the world have also shown that the assumptions used to derive the present VIS model may not be globally valid. This provides the basis for further investigation, especially in the context of the subsurface extent of Precambrian provinces, the composition of the lower crust and the crustal thickness of a region. We know that exposed Precambrian rocks constitute only 29% of the total Precambrian crust [Goodwin, 1991]. This indicates that a significant portion of the Precambrian crust on the continents is overlain by younger Phanerozoic cover. Hence one of aims of the present study is to look for possible extensions of the Precambrian provinces under the Phanerozoic cover and possibly redefine the subsurface boundaries of these provinces. Following up on the disagreements between the predicted and the observed anomaly maps, we select regions for further study. On the basis of the results from different geophysical methods, the subsurface boundary of the Precambrian province to be studied is modified and the VIS value recomputed. Using this new VIS model, the vertical field anomaly map is computed at satellite altitude and the iteration repeated until a reasonable

Table 2. Geological Regions Over Continents and Oceans Showing Possible Reasons for Disagreement Between Observed and Predicted Anomalies^a

Geological Region	Location on the Map of Figure 12 ^b	Likely Reasons for Misfit
<i>Continental Regions</i>		
Tarim Basin	1	B
Songliao microcontinent	2	A
Tibetan Plateau	3	D
Myanmar region	4	E
Eastern Dharwar region	5	E
Khatanga Trough	6	B
Eastern region of Koylma-Omolon block	7	A, B
East European Craton	8, 9, 10, 11	D, G
Newfoundland	12	A, B
Mackenzie mountains	13	B, E
Kentucky-Tennessee region	14	A
Bahamas	15	E
San Francisco Belt	16	A, B
Ribeira Belt	17	A, B
Amsaga Shield	18	C, E, F
Liberian Shield	19	C, E, F
Arabian Shield	20	B, E
Bangui region	21	D, E
Angolan Craton	22	E
Kaapvaal Craton	23	B
Zimbabwe Craton	24	C
Pilbara Craton	25	H
Hamersley Basin	26	E
McArthur Basin	27	E
Central Greenland	28	D
<i>Oceanic Regions</i>		
Faeroe-Rockall Plateau	29	A, C
Broken Ridge	30	G
Hess Rise	31	E, G
Hawaiian Ridge	32	E, G
Ontong-Java Plateau	33	A, C
Lord Howe Rise	34	A, C, G
North Atlantic Ocean		F
Central Atlantic Ocean		F, I
South of Australia, Indian Ocean	35	I, J
Pacific Ocean		I, J

^aPossible causes for these disagreements are geological boundary location (A), existence of craton beneath cover (B), thicker/thinner crust (C), Curie isotherm variation (D), high magnetization of lower crust (E), magnetization extending into the upper mantle (F), dominant remanent magnetization (G), high estimated VIS value over the region (H), unfiltered external field (I), and presence of short wavelengths of the Earth's main field (J).

^bNumbers are shown in Figure 12.

fit is achieved with the observed anomaly map. The computations are done using the same forward modeling procedure as described earlier in section 2. Four regions in different tectonic settings are studied. The first region of our study is northern Greenland, largely to infer the crustal structure and hidden geology based on the strength of the observed magnetic anomaly. The thickness of the magnetic crust of the West African Craton is investigated next. The third region of study is the Bangui anomaly in the central African region. The composition of the lower crust is inferred in this region. Finally, the magnetic signature of the deformed Koylma Block, located in the eastern region of Siberia, is investigated.

4.3.1. Northern Greenland

[33] The observed vertical field anomaly map over Greenland (Figure 13a) shows an anomaly trending in the

NE-SW direction across the center of northern Greenland. As discussed in section 4.2 the initial model vertical field anomaly over northern Greenland (Figure 13b) shows a disagreement with the observations. This discrepancy cannot be resolved readily because more than 90% of Greenland is under a cover of thick ice. Recent geophysical studies over Greenland have provided new insights into the nature of the crust below the ice cover [Dahl-Jensen *et al.*, 2003]. Dahl-Jensen *et al.* have derived seismic Moho depth variations for Greenland (Figure 13d). A possible boundary of Proterozoic in age separating the northern and southern blocks of Greenland was inferred using these results [Dahl-Jensen *et al.*, 2003]. The boundary, as shown in Figure 13d as a dashed line, extends in the northeast direction from the western flank of the Naggastoquidian Belt toward the eastern coast of Greenland. Assuming the block south of this boundary to have a lower susceptibility (0.0204 SI) than the northern block (0.0404 SI), the predicted anomaly is displayed in Figure 13c. While the elongated anomaly feature trending NE-SW in the observed map is not completely reproduced in the first iteration map it shows a better agreement with the observations. The anomalies for the initial model, first iteration model and the observed map along the profile section AA' are shown in Figure 13e. The curves show a good fit between the first iteration prediction and the observed anomaly, indicating that there may indeed be a boundary separating two blocks of different composition.

4.3.2. West African Craton, West Africa

[34] The observed anomaly map (Figure 14a) shows a band of negative anomalies that extend over the Liberian Shield with a strong positive observed over the Kasila series (Figure 14d). A positive anomaly of high amplitude is observed over the western Taoudeni Basin south of Amsaga Archean belt. Largely, the predicted anomaly patterns (Figure 14b) over the West African Craton are in agreement with the observed patterns. The strength of the predicted anomaly is too low, though, and the shapes differ over the north Taudeni Basin. The tectonic map of the West African Craton is shown in Figure 14d. The Archean rocks of the Amsaga belt (Reguibat Shield) in the north and the Liberian Shield in the south, including the exposed Kasila series, are composed of mafic rock types [Goodwin, 1991]. The VIS values for these regions are derived on the basis of these exposed rock types [Hemant, 2003].

[35] The general lack of strength in the predicted amplitude for this region may be due to the 3SMAC model underestimating the thickness of Archean crust in the West African cratonic region. The thickness given by 3SMAC model for Amsaga Archean belt is 32–35 km and for the Liberian shield is 30–33 km. However, the crustal thickness for Archean provinces and other shield regions, in general, is greater than 40 km [Bassin *et al.*, 2000]. In South Africa, it is 35–45 km [Nguuri *et al.*, 2001]. It is even claimed that the crust in the south of the West African Craton is 70 km thick [Toft and Haggerty, 1988]. The temperature map of Artemieva and Mooney [2001], supports the hypothesis of a thicker crust. We increase the modeled thickness of crust in the Amsaga belt and Liberian shield by a moderate 8.0 km, which is well within the uncertainties of 3SMAC for this region. Additionally, we extend the geological boundary of the buried Amsaga belt further south below the basin. The

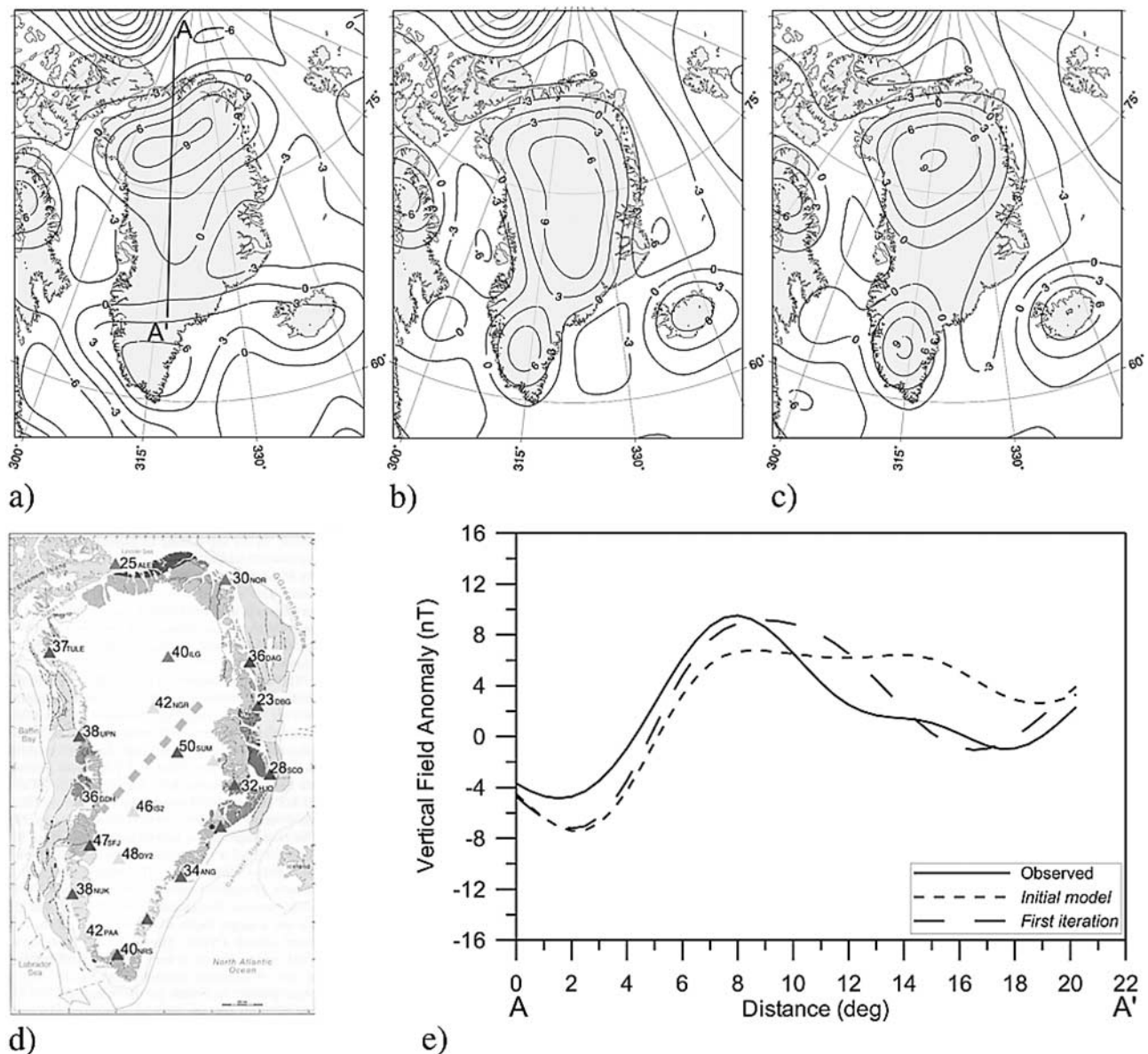


Figure 13. (a) Observed vertical field anomaly map for spherical harmonic degrees 16–90 at an altitude of 400 km for Greenland, the same map (b) for initial model and (c) for the first iteration. (d) Depths to Moho in km for all the seismic stations. The suggested division of the Proterozoic part of Greenland is marked as dashed line [Dahl-Jensen *et al.*, 2003] (with permission from Elsevier). (e) Profile sections along AA' shown in Figure 13a.

geological map for the West African Craton (Figure 14e) shows the redefined boundary of Amsaga belt as a white line. The recomputed first iteration map shown in Figure 14c now shows a stronger anomaly pattern over the West African Craton and agrees better with the observed field over the western Taudeni Basin. The profile across the craton (Figure 14f) shows the amplitudes of the anomalies of the observed anomaly map along with the initial and first iteration model. Discrepancies of 1.5–2.5 nT are yet unaccounted for, especially over the shield regions of the craton. Either the crust is still thicker in the region or magnetization may extend into the upper mantle [Toft *et al.*, 1992].

4.3.3. Bangui Anomaly, Central Africa

[36] The central African region has one of the most prominent magnetic anomalies at satellite altitude (Figure 15a).

While our initial model (Figure 15b) is in agreement with the observations on the shape of the anomaly, it severely underestimates its amplitude. To account for the missing strength, we concentrate on the composition and susceptibility of the lower crust. The map of central Africa (Figure 15d) shows the geological setup of the region north of the Congo Craton. This region witnessed Pan-African orogenesis (800–530 Ma) resulting in the intrusion of the Oubanguides in the region north of Bangui where it is exposed and along the entire stretch north of the Congo Craton [Pin and Poidevin, 1987]. Figure 15d shows the distribution of granulites in the northern part of the Congo Craton. The high content of iron oxides in two of three samples of granulite [Pin and Poidevin, 1987] suggests that they can only be derived from a more mafic parental magma

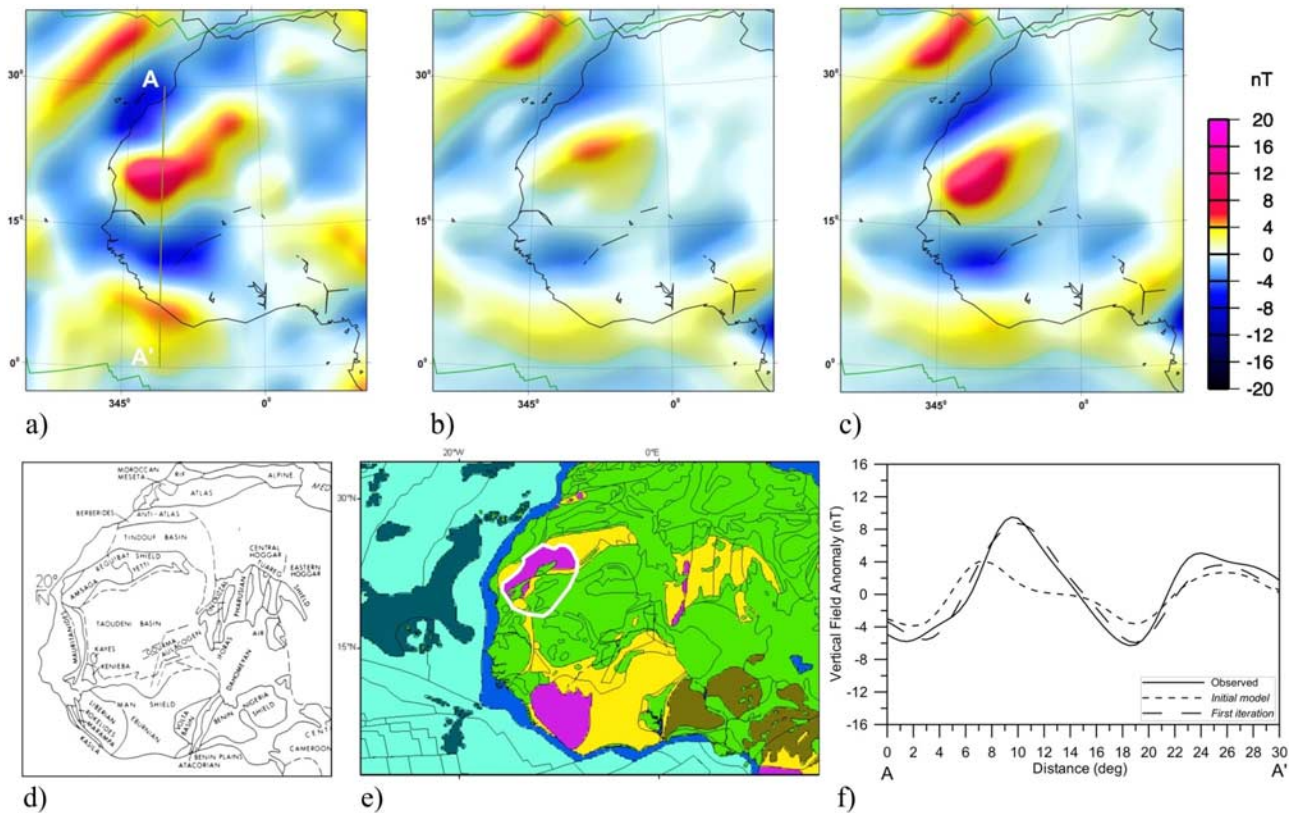


Figure 14. (a) Observed vertical field anomaly map for spherical harmonic degrees 16–90 at an altitude of 400 km for West African region, the same map (b) for initial model and (c) for the first iteration. (d) Tectonic map of the West African region [Goodwin, 1991] (with permission from Elsevier). (e) Geological map of the West African region. Thin black line is the previous boundary and the thick white line marks the new boundary of the subsurface extension of the Amsaga belt. The colors represent the geological units mentioned in Figure 1. (f) Profile section along AA', marked in Figure 14a.

[Chappell *et al.*, 1988; Clark, 1999]. However, the bulk susceptibility of the rock types exposed in the region falls short of the total susceptibility required to reproduce the Bangui anomaly. Following, the work of Pin and Poidevin [1987] the lower crust of the central African region is considered to be of a more mafic composition than inferred on the basis of surface geology. Emplacement of basalts in the lower crust as a result of the Pan-African orogeny is a possibility.

[37] By assigning a basaltic composition to the lower crust and parts of the upper crust in the region occupied by granulites north of the Congo Craton, the predicted first iteration magnetic anomaly map (Figure 15c) for the region now is able to account for most of the missing amplitude. Profile BB' across the Bangui anomaly (Figure 15e) shows the amplitude of the first iteration and the observed anomaly. The amplitudes agree well in the northern half of the profile. Over the southern half, the anomaly difference reaches 2–3 nT. These results are in agreement with Regan and Marsh [1982], who considered the source for the Bangui anomaly to be geological in origin. They modeled the anomaly by assuming the entire crust below Bangui to be mafic in composition, having susceptibility value of 0.13 SI units higher than the surrounding. A more felsic lower crust below the Congo Craton or remanent magnetization component in the direction of the induced field could

explain the missing anomaly in the southern lobe. A deeper Curie isotherm below Bangui in the northern region and an elevated Curie isotherm beneath the Congo Craton could also possibly account for the missing amplitude. Indeed, the temperature distribution map at the depth of 50 km prepared by Artemieva and Mooney [2001] supports this argument. Ravat [1989] modeled the Bangui anomaly by considering a 3.0 km thick block with a susceptibility of 1.0 SI, which would be unusually high for a geological body. The upper crust of the surrounding region was considered felsic while the lower crust was considered more mafic. They proposed a nongeological origin of the anomaly, possibly an iron or iron-nickel meteorite. Following on the same lines, Girdler *et al.* [1992] proposed an iron meteorite as the source of the Bangui anomaly. Our results indicate, however, that it is not necessary to invoke an extraterrestrial body to explain the Bangui anomaly.

4.3.4. Kolyma-Omolon Block, Siberia

[38] Geological provinces in the eastern region of Siberia comprise mostly accreted regions [Fujita, 1978; Churkin and Trexler, 1980], including the Kolyma and Omolon blocks. The region of the Kolyma-Omolon Block is mostly buried, apart from a few outcrops along the Cherskiy suture zone. The tectonic activity of the region before and after the collision of the Brooks-Chukotsk block with East Siberia and western Alaska [Sweeney, 1981; Howell and Wiley,

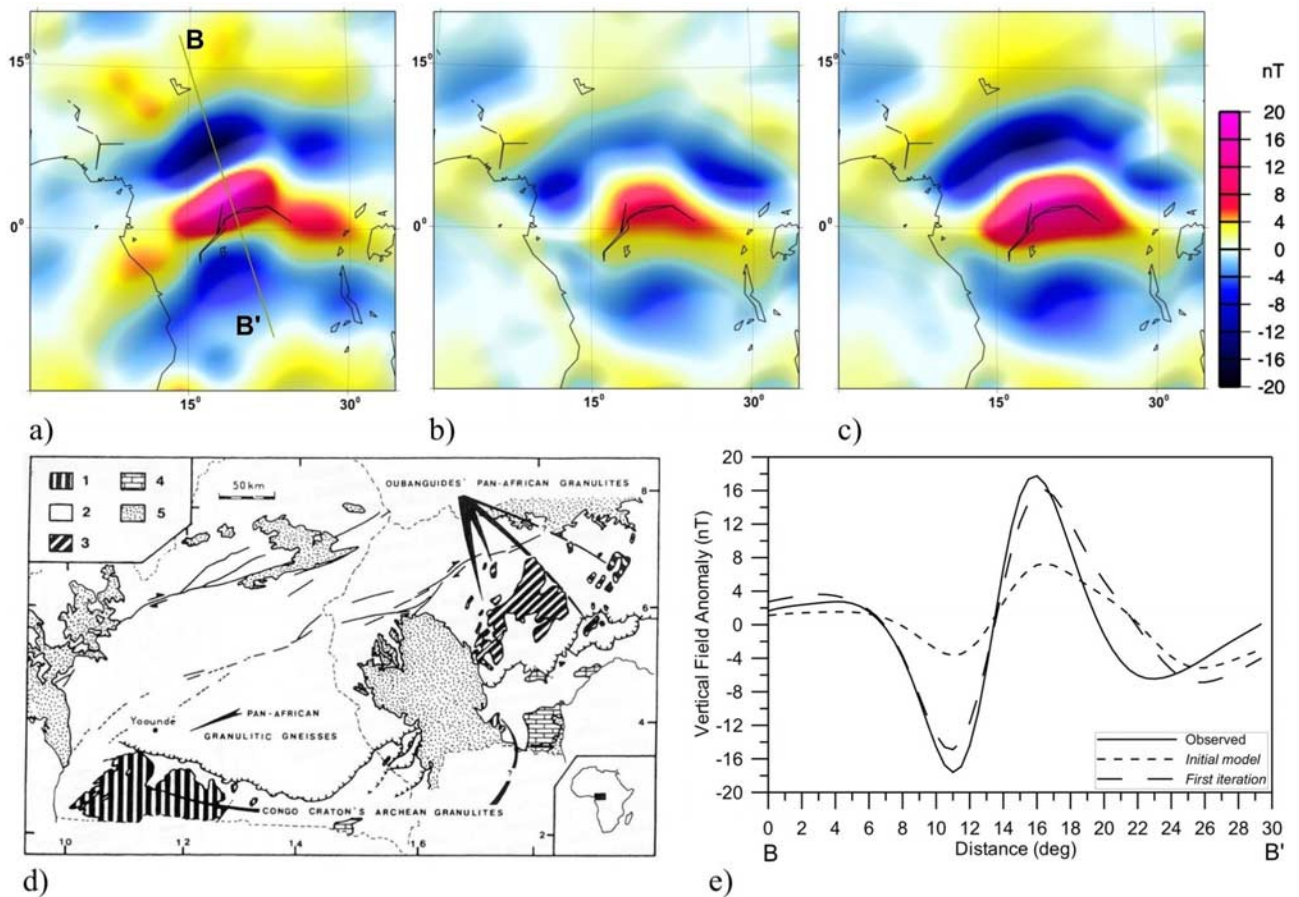


Figure 15. (a) Observed vertical field anomaly map for spherical harmonic degrees 16–90 at an altitude of 400 km for the central African region, the same map (b) for the initial model and (c) the first iteration model. (d) Granulites distribution of the northern part of Congo Craton [Pin and Poidevin, 1987] (with permission from Elsevier). 1, Archean granulates; 2, undifferentiated Precambrian formations; 3, Pan-African granulates; 4, sedimentary upper Precambrian foreland of Oubanguides; 5, post-Pan-African cover. (e) Profile section along BB' marked in Figure 15a.

1987], respectively, is shown in Figures 16a–16d. The shape of the Kolyma Block during the early Jurassic period is shown in Figure 16a, and until early Tertiary (Figure 16d) it was assumed to have remained the same. On the basis of the suggested shape of the Kolyma block, the predicted anomaly (Figure 17b) does not match the observed field (Figure 17a). We investigate here the source for the observed anomaly, whose shape follows the Cherskiy suture zone.

[39] Following the tectonic history of the Kolyma Block [Sweeney, 1981; Howell and Wiley, 1987] and the intraplate processes that wrenched and internally rotated the Brooks-Chukotsk block on both sides of the Bering Sea, it is hard to envisage that the Kolyma Block would not have been deformed. Considering that during the late Cretaceous and early Tertiary era, when the Chukotsk block collided with the Kolyma Block forming the Anyui suture, it compressed the Kolyma Block against the Cherskiy suture zone. This also caused deformation in the Verkhoyansk fold belt located west of the Kolyma and Cherskiy suture zones. Further, as the Chukotsk block rotated internally in an anticlockwise direction, this could have caused the Kolyma Block to deform and extend along the eastward direction.

The boundary of this deformed Kolyma Block, which is partially overlain by the Phanerozoic sediments in the region, is retraced here, following the observed anomaly pattern over the region. The deformed block is shown as shaded region in Figure 16d. The VIS value for the block is recomputed for this new boundary keeping the susceptibility value constant. The predicted first iteration anomaly map (Figure 17c) associated with the new boundary of the Kolyma Block now agrees well with the observations (Figure 17a). The profile section across the region provides a numerical estimate for the observed and the predicted anomaly maps and is shown in Figure 17d. The curves show a significant improvement over the initial model. The magnetic anomaly study in this region demonstrates the ability of the GIS based modeling method to trace the subsurface extension of a buried and deformed block.

4.4. Global First Iteration Model

[40] The interpretation of the initial model and the observed anomaly maps demonstrated that most of the observed anomalies are geological in origin and can be explained by a simple model incorporating only induced magnetization. For selected regions, we revisited the source

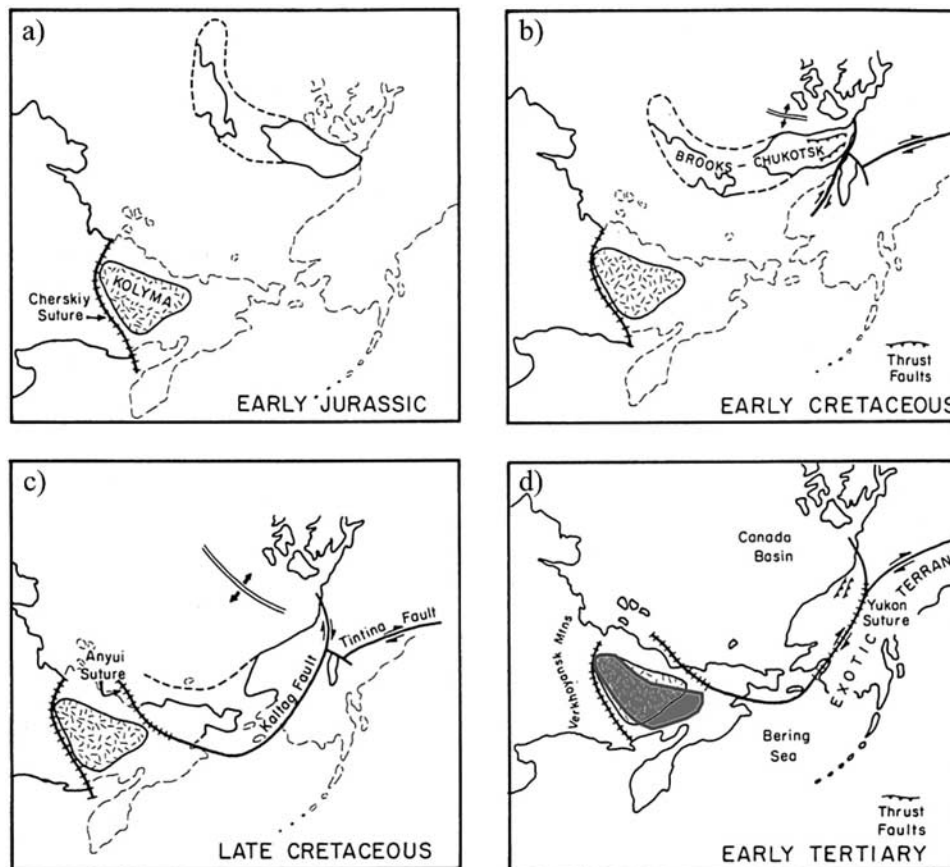


Figure 16. Tectonic reconstruction of the Cordilleran Arctic region since the Early Jurassic [Sweeney, 1981; Howell and Wiley, 1987]. Diagram is taken from *Condie* [1989] (with permission from Elsevier). The shaded region shown in gray color in Figure 16d marks the new boundary of the deformed Kolyma block and is used in deriving first iteration VIS model.

geology and adapted it to the observed anomalies. This leads to considerable reductions in the misfit for the continental regions, namely northern Greenland, western Africa, central Africa, Kolyma Block in Siberia, central US and Tarim Craton in China. The predicted global vertical field anomaly map for this first iteration model, is computed is shown in Figure 18. It shows a significant improvement over the initial prediction (Figure 7) in the shape and amplitude of anomalies for the revisited regions.

5. Conclusions

[41] The aims of this study were to interpret crustal magnetic anomalies observed at satellite altitude and to prove that quantitative geological information can be extracted from them by varying the subsurface boundaries of Precambrian provinces overlain by Phanerozoic sediments and sometimes changing their presumed composition. For this purpose, a new and efficient way to model the geological units and their crustal structure on a GIS platform was developed. A global vertically integrated susceptibility model was derived based on an average susceptibility value for the various geological regions of the continents and oceans. To explain anomalies over the oceans, remanent magnetization was included in the model. The overall agreement in the predicted and observed

magnetic anomaly maps indicates that the sources of the magnetic anomalies are indeed geological in origin and lie in the Earth's crust. This also supports our assumptions employed during the derivation of the global VIS and VIM maps. The magnetization model used here reproduces most of the magnetic anomalies observed at satellite altitude.

[42] The flexibility offered by the GIS based modeling method to easily change the shape of a geological province assisted in the detailed study of the Precambrian provinces. Modifying the presumed boundaries of buried parts of the Precambrian provinces in selected regions led to the derivation of a first iteration VIS model. This approach could be extended to many such regions to redefine the boundaries of the Precambrian provinces hidden below the young crust.

[43] For the derivation of the VIS model, the lower crust was assumed to be 1.2 times more magnetic than the corresponding upper crust of Archean in age and 1.6 times more magnetic for the upper crust of post-Archean in age. As the composition of the lower crust is at present largely speculative, based on xenolith data [Haggerty, 1978] or exposed portions of the lower crust [Fountain and Salisbury, 1981], the composition of the lower crust need not be consistent with the upper crust [Chappell et al., 1988] as assumed in this paper. Thus the lower crust in some regions of the world can have significantly different

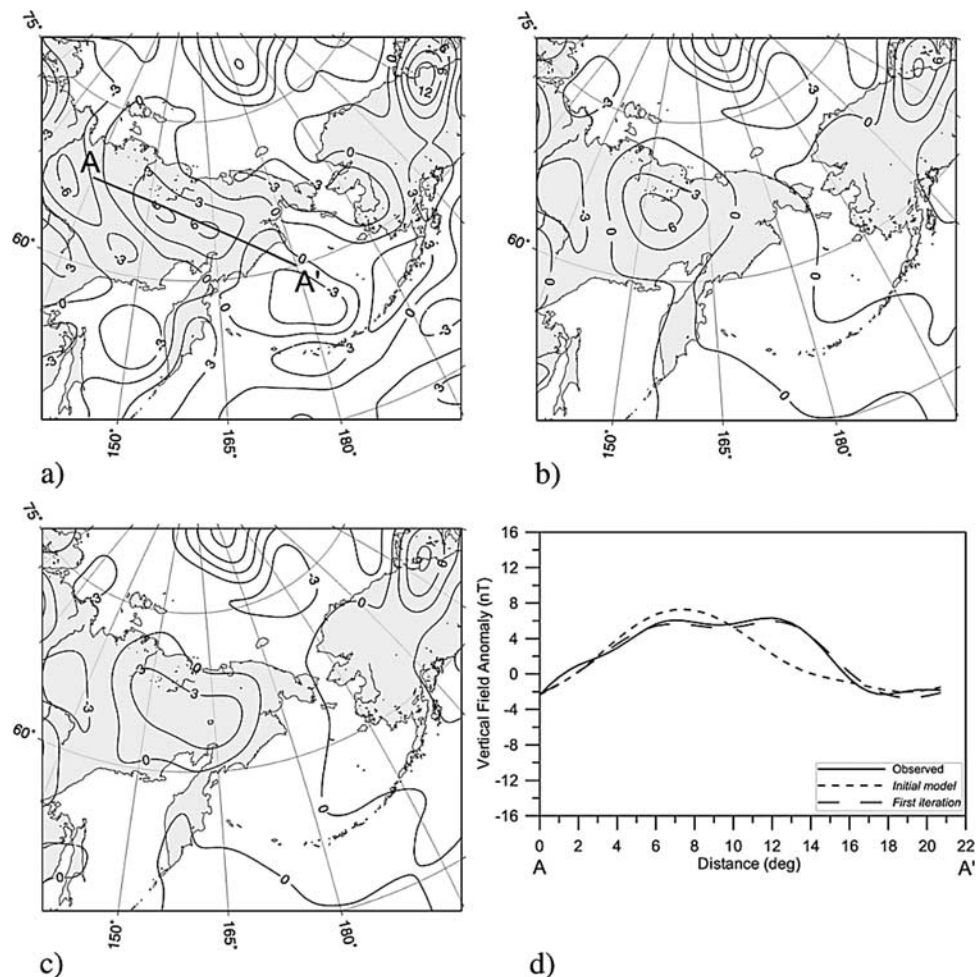


Figure 17. (a) Observed vertical field anomaly map for spherical harmonic degrees 16–90 at an altitude of 400 km for Kolyma block, the same map (b) for the initial model and (c) for the first iteration model. (d) Profile section along AA' marked in Figure 17a.

magnetic properties than the corresponding upper part of the crust. For instance, a mafic lower crust, basically basaltic in composition, can explain the source for the observed strong anomaly over Bangui. For the West African Craton, the modeling result suggests a thicker crust in the region, in agreement with the results of *Toft et al.* [1992]. However, magnetization extending into the upper mantle and the effect of variation in Curie isotherm cannot be ruled out in this region. The results for Africa suggest that the variation in the crustal thickness can be an important cause for variation in the strength of anomalies.

[44] Remanent magnetization does not appear to be important in modeling continental anomalies, except, perhaps, over the East European Craton. Over the oceans, predicted anomalies using both induced and remanent magnetization as the sources show significant agreement with the observed anomalies. Some disagreement persists over the Pacific Ocean. Oceanic plateaus are modeled here using just induced magnetization as the source. Largely, predicted anomalies show a good agreement with observations. However, the partial disagreement between the predicted and the observed anomaly over the Faeroe-Rockall Plateau, Broken Ridge, the Hess Rise, region north of the

Hawaiian ridge and the Lord Howe Rise suggests that remanent magnetization could be an additional source of the observed anomalies in these areas.

[45] The difference between the initial prediction and the observed anomalies (Figure 12) shows large discrepancies indicating that additional sources like variation in the depth of the Curie isotherm, remanent magnetization over the continents and oceans need to be incorporated in further studies to explain the cause of these anomalies. The disagreements also point to our limited knowledge about the subsurface geology and composition of the crust.

[46] Having established that the anomalies can be modeled and predicted assuming a simple geological model using nonsatellite information, this should provide a new basis for interpreting increasingly accurate satellite data measured by the CHAMP satellite from steadily decreasing orbital altitudes. The forgoing interpretations of individual observed anomalies using the present modeling method show the way for an increased use of satellite magnetic anomalies for the study of the crust and the lithosphere. The upcoming three-satellite mission swarm (<http://www.esa.int/esaLP/LPswarm.html>) is expected to yield even more accurate high-resolution crustal magnetic anomaly maps, which

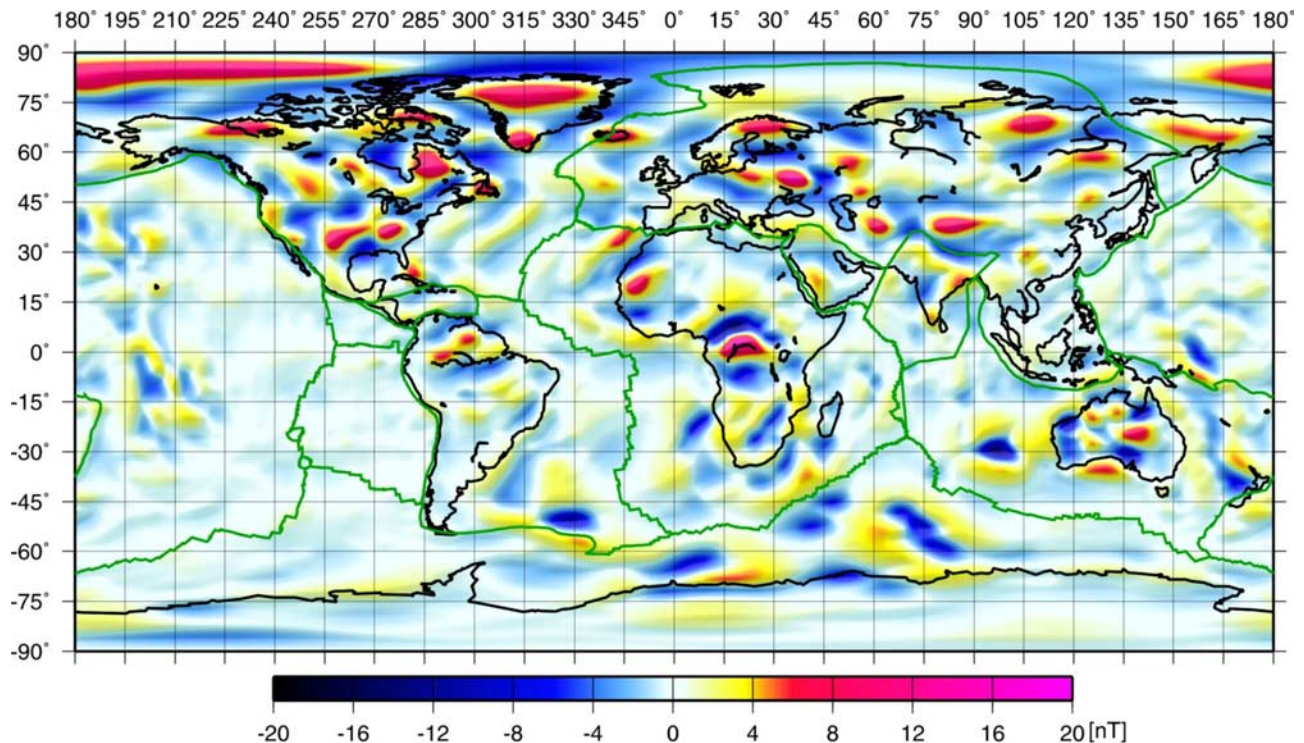


Figure 18. First iteration vertical field anomaly map for spherical harmonic degrees 16–90 at an altitude of 400 km.

should make it possible to further delineate the small geological provinces which are already part of the present GIS based modeling method.

[47] **Acknowledgments.** We thank Phil Wannamaker, Randy Enkin, Mark Pilkington, Kevin Mickus and an anonymous reviewer for going through the manuscript in detail and providing constructive comments to improve the quality of the manuscript. Figures 5, 7, 8, 12, 13, 14, 16, 17, and 18 are prepared using GMT [Wessel and Smith, 1998]. We also thank the group members from the CHAMP mission for providing the processed data and the technical support without which this work would not have materialized.

References

- Achache, J., A. Abtout, and J. L. LeMouél (1987), The downward continuation of Magsat crustal anomaly field over Southeast Asia, *J. Geophys. Res.*, *92*, 11,584–11,596.
- Arkani-Hamed, J. (1991), Thermoremanent magnetization of the oceanic lithosphere inferred from a thermal evolution model: Implications for the source of marine magnetic anomalies, *Tectonophysics*, *192*, 81–96.
- Arkani-Hamed, J., and D. W. Strangway (1986), Effective magnetic susceptibility anomalies of the oceanic upper mantle derived from Magsat data, *Geophys. Res. Lett.*, *13*, 999–1002.
- Arkani-Hamed, J., R. A. Langel, and M. E. Purucker (1994), Magnetic anomaly maps of Earth derived from POGO and Magsat data, *J. Geophys. Res.*, *99*, 24,075–24,090.
- Artemieva, I. M., and W. D. Mooney (2001), Thermal thickness and evolution of Precambrian lithosphere: A global study, *J. Geophys. Res.*, *106*, 16,387–16,414.
- Bassin, C., G. Laske, and G. Masters (2000), The current limits of resolution for surface wave tomography in North America, *Eos Trans AGU*, *81*(48), Fall Meet Suppl., Abstract S12A-03.
- Berckhemer, H., et al. (1997), Petrophysical properties of the 9-km-deep crustal section at KTB, *J. Geophys. Res.*, *102*, 18,337–18,362.
- Blakely, R. G. (1995), *Potential Theory in Gravity and Magnetic Applications*, Cambridge Univ. Press, New York.
- Blakely, R. J., and A. Griscom (1988), Geologic insights from upward continuation and boundary analysis of North American magnetic and gravity maps, *Geol. Soc. Am. Abstr. Programs*, *20*, A325.
- Blakely, R. J., R. E. Wells, T. S. Yelin, I. P. Madin, and M. H. Beeson (1995), Tectonic setting of the Portland-Vancouver area, Oregon and Washington: Constraints from low-altitude aeromagnetic data, *Geol. Soc. Am. Bull.*, *107*, 1051–1062.
- Butler, R. F. (1992), *Paleomagnetism: Magnetic Domains to Geologic Terranes*, Blackwell Sci., Malden, Mass.
- Cain, J. C., Z. Wang, C. Kluth, and D. R. Schmitz (1989), Derivation of a geomagnetic model to $n = 63$, *Geophys. J.*, *97*, 431–441.
- Cande, S. C., and D. V. Kent (1995), Revised calibration of the geomagnetic polarity timescale for the Late Cretaceous and Cenozoic, *J. Geophys. Res.*, *100*, 6093–6096.
- Carlson, R. L., N. I. Christensen, and R. P. Moore (1980), Anomalous crustal structure in ocean basins: Continental fragments and oceanic plateaus, *Earth Planet. Sci. Lett.*, *51*, 171–180.
- Chappell, B. W., A. J. R. White, and R. Hine (1988), Granite provinces and basement terranes in the Lachlan Fold Belt, southeastern Australia, *Aust. J. Earth Sci.*, *35*, 505–521.
- Churkin, M., Jr., and J. H. Trexler (1980), Circum-Arctic plate accretion-Isolating part of the Pacific plate to form the nucleus of the Arctic basin, *Earth Planet. Sci. Lett.*, *48*, 356–362.
- Clark, D. A. (1999), Magnetic petrology of igneous intrusions: Implications for exploration and magnetic interpretation, *Explor. Geophys.*, *30*, 5–26.
- Clark, D. A., and D. W. Emerson (1991), Notes on rock magnetization characteristics in applied geophysical studies, *Explor. Geophys.*, *22*, 547–555.
- Clark, S. C., H. Frey, and H. H. Thomas (1985), Satellite magnetic anomalies over subduction zones: The Aleutian arc anomaly, *Geophys. Res. Lett.*, *12*, 41–44.
- Cohen, Y., and J. Achache (1994), Contribution of induced and remanent magnetization to long-wavelength oceanic magnetic anomalies, *J. Geophys. Res.*, *99*, 2943–2954.
- Commission for the Geological Map of the World (CGMW) (2000), Geological map of the World, UNESCO, Paris.
- Condie, K. C. (1989), *Plate Tectonics and Crustal Evolution*, 244–282 pp., Elsevier, New York.
- Counil, J.-L., and J. Achache (1987), Magnetization gaps associated with tearing in the central America subduction zone, *Geophys. Res. Lett.*, *14*, 1115–1118.
- Cox, A., and R. B. Hart (1986), *Plate Tectonics: How It Works*, 392 pp., Blackwell Sci., Malden, Mass.

- Dahl-Jensen, T., T. B. Larsen, I. Woelbern, T. Bach, W. Hanka, R. Kind, S. Gregersen, K. Mosegaard, P. Voss, and O. Gudmundsson (2003), Depth to Moho in Greenland: Receiver-function analysis suggests two Proterozoic blocks in Greenland, *Earth Planet. Sci. Lett.*, *205*, 379–393.
- Dyment, J., and J. Arkani-Hamed (1998), Contribution of lithospheric remanent magnetization to satellite magnetic anomalies over the world's oceans, *J. Geophys. Res.*, *103*, 15,423–15,441.
- Fountain, D. M., and M. H. Salisbury (1981), Exposed crustal-sections through the continental crust: Implications for crustal structure, petrology and evolution, *Earth Planet. Sci. Lett.*, *56*, 263–277.
- Frey, H. (1982), Magsat scalar anomalies and major tectonic boundaries in Asia, *Geophys. Res. Lett.*, *9*, 299–302.
- Frey, H. (1985), Magsat and POGO magnetic anomalies over the Lord Howe Rise: Evidence against a simple continental crustal structure, *J. Geophys. Res.*, *90*, 2631–2639.
- Frost, B. R., and P. N. Shive (1986), Magnetic mineralogy of the lower continental crust, *J. Geophys. Res.*, *91*, 6513–6522.
- Fujita, K. (1978), Pre-Cenozoic tectonic evolution of northeast Siberia, *J. Geol.*, *86*, 159–172.
- Fullerton, L. G., H. V. Frey, J. H. Roark, and H. H. Thomas (1994), Contributions of Cretaceous quite zones natural remanent magnetization to Magsat anomalies in the southwest Indian Ocean, *J. Geophys. Res.*, *99*, 11,923–11,936.
- Girdler, R. W., P. T. Taylor, and J. J. Frawley (1992), A possible impact origin for the Bangui magnetic anomaly (central Africa), *Tectonophysics*, *212*, 45–58.
- Goodwin, A. M. (1991), *Precambrian Geology*, Elsevier, New York.
- Goodwin, A. M. (1996), *Principles of Precambrian Geology*, Elsevier, New York.
- Gradstein, F. M., F. P. Agterberg, J. G. Ogg, J. Hardenbol, P. van Veen, J. Thierry, and Z. Huang (1994), A Mesozoic time scale, *J. Geophys. Res.*, *99*, 24,051–24,074.
- Haggerty, S. E. (1978), Mineralogical constraints on Curie isotherms in deep crustal magnetic anomalies, *Geophys. Res. Lett.*, *5*, 105–108.
- Hahn, A., H. Ahrendt, J. Jeyer, and J.-H. Hufen (1984), A model of magnetic sources within the Earth's crust compatible with the field measured by the satellite Magsat, *Geol. Jahrb., Reihe A*, *75*, 125–156.
- Hall, D. H. (1974), Long-wavelength aeromagnetic anomalies and deep crustal magnetisation in Manitoba and northwestern Ontario, Canada, *J. Geophys.*, *40*, 403–430.
- Hayling, K. L., and C. G. A. Harrison (1986), Magnetization modeling in the north and equatorial Atlantic Ocean using Magsat data, *J. Geophys. Res.*, *91*, 12,423–12,443.
- Hemant, K. (2003), Modelling and interpretation of global lithospheric magnetic anomalies, Ph.D. thesis, Freie Univ., Berlin.
- Hemant, K., and S. Maus (2005), Why no anomaly is visible over most of the continent-ocean boundary in the global crustal magnetic field, *Phys. Earth Planet. Inter.*, *149*, 321–333.
- Howell, D. G., and T. J. Wiley (1987), Crustal evolution of northern Alaska inferred from sedimentology and structural relations of the Kandik area, *Tectonics*, *6*, 619–631.
- Hunt, C. P., B. M. Moskowitz, and S. K. Banerjee (1995), Magnetic properties of Rocks and Minerals, in *Rock Physics and Phase Relations: A Handbook of Physical Constants, AGU Ref. Shelf*, vol. 3, edited by T. J. Ahrens, pp. 189–204, AGU, Washington, D. C.
- Kearey, P., and F. J. Vine (1990), *Global Tectonics*, Blackwell, Malden, Mass.
- LaBrecque, J. L., and C. A. Raymond (1985), Seafloor spreading anomalies in the Magsat field of the North Atlantic, *J. Geophys. Res.*, *90*, 2565–2575.
- Langel, R. A., G. Ousley, and J. Berbert (1982), The Magsat Mission, *Geophys. Res. Lett.*, *9*, 243–245.
- Laske, G., and G. Masters (1997), A global digital map of sediment thickness (abstract), *Eos Trans. AGU*, *78*(46), Fall Meet. Suppl., F483.
- Maus, S., M. Rother, R. Holme, H. Lühr, N. Olsen, and V. Haak (2002), First scalar magnetic anomaly map from CHAMP satellite data indicates weak lithospheric field, *Geophys. Res. Lett.*, *29*(14), 1702, doi:10.1029/2001GL013685.
- Maus, S., R. Martin, K. Hemant, S. Claudia, H. Luehr, A. Kuvshinov, and N. Olsen (2005), Earth's crustal magnetic field determined to spherical harmonic degree 90 from CHAMP satellite measurements, *Geophys. J. Int.*, in press.
- McEnroe, S. A., F. Langenhorst, P. Robinson, G. D. Bromiley, and C. S. J. Shaw (2004), What is magnetic in the lower crust?, *Earth Planet. Sci. Lett.*, *226*, 175–192.
- Meyer, J., J.-H. Hufen, M. Siebert, and A. Hahn (1983), Investigations of the internal geomagnetic field by means of a global model of the Earth's crust, *J. Geophys. Res.*, *52*, 71–84.
- Müller, R. D., W. R. Roest, J.-Y. Royer, L. M. Gahagan, and J. G. Sclater (1997), Digital isochrons of the world's ocean floor, *J. Geophys. Res.*, *102*, 325–338.
- Nataf, H.-C., and Y. Ricard (1996), 3SMAC: An a priori tomographic model of the upper mantle based on geophysical modelling, *Phys. Earth Planet. Inter.*, *95*, 101–122.
- Nguuri, T. K., J. Gore, S. J. Webb, C. Wright, T. G. Zengeni, O. Gwavava, J. A. Snoke, and Kaapvaal Seismic Group (2001), Crustal structure beneath southern Africa and its implications for the formation and evolution of the Kaapvaal and Zimbabwe cratons, *Geophys. Res. Lett.*, *28*, 2501–2504.
- Nur, A., and Z. Ben-Avraham (1982), Oceanic plateaus, the fragmentation of continents, and mountain building, *J. Geophys. Res.*, *87*, 3644–3661.
- Olsen, N., et al. (2000), Orsted initial field model, *Geophys. Res. Lett.*, *27*, 3607–3610.
- Pilkington, M., and J. A. Percival (1999), Crustal magnetization and long wavelength aeromagnetic anomalies of the Minto block, Quebec, *J. Geophys. Res.*, *104*, 7513–7526.
- Pin, C., and J. L. Poidevin (1987), U-Pb Zircon evidence for a Pan-African granulite facies metamorphism in the central African Republic: A new interpretation of the high-grade series of the northern border of the Congo craton, *Precambrian Res.*, *36*, 303–312.
- Pohl, J., T. Pätzold, C. Rolf, H. C. Soffel, and H. U. Worm (1991), A rock magnetic log of the KTB pilot borehole, *Sci. Drill.*, *2*, 120–129.
- Prol-Ledesma, R. M. (2000), Evaluation of the reconnaissance results in geothermal exploration using GIS, *Geothermics*, *29*, 83–103.
- Pucher, R., and T. Wonik (1998), A new interpretation of the Magsat anomalies of central Europe, *Phys. Chem. Earth*, *23*, 981–985.
- Purucker, M. E., and J. Dyment (2000), Satellite magnetic anomalies related to sea floor spreading in the South Atlantic Ocean, *Geophys. Res. Lett.*, *27*, 2765–2768.
- Purucker, M. E., R. A. Langel, M. Rajaram, and C. Raymond (1998), Global magnetization models with a priori information, *J. Geophys. Res.*, *103*, 2563–2584.
- Purucker, M., B. Langlais, N. Olsen, G. Hulot, and M. Manda (2002), The southern edge of cratonic North America: Evidence from new satellite magnetometer observations, *Geophys. Res. Lett.*, *29*(15), 8000, doi:10.1029/2001GL013645.
- Ravat, D., R. A. Langel, M. Purucker, J. Arkani-Hamed, and D. E. Alsdorf (1995), Global vector and scalar Magsat magnetic anomaly maps, *J. Geophys. Res.*, *100*, 20,111–20,136.
- Ravat, D. N. (1989), Magsat investigations over the greater African region, Ph.D. thesis, Purdue Univ., West Lafayette, Ind.
- Raymond, C. A., and J. L. LaBrecque (1987), Magnetization of the oceanic crust: Thermoremanent magnetization or chemical remanent magnetization?, *J. Geophys. Res.*, *92*, 8077–8088.
- Reeves, C. V., and M. de Wit (2000), Making ends meet in Gondwana: Retracing the transforms of the Indian Ocean and reconnecting continental shear zones, *Terra Nova*, *12*, 272–280.
- Regan, R. D., and B. D. Marsh (1982), The Bangui magnetic anomaly: Its geological origin, *J. Geophys. Res.*, *87*, 1107–1120.
- Regan, R. D., J. C. Cain, and W. M. Davis (1975), A global magnetic anomaly map, *J. Geophys. Res.*, *80*, 794–802.
- Rosenbaum, M. S., and C. P. Nathanail (1996), Petrophysical databases for ground characterisation: Design concepts and considerations, *Mar. Pet. Geol.*, *13*, 427–435.
- Royer, J. Y., R. D. Müller, L. M. Gahagan, L. A. Lawver, C. L. Mayes, D. Nuerberg, and J. G. Sclater (1992), A global isochron chart, *Tech. Rep. 117*, 38 pp., Inst. for Geophys., Univ. of Tex., Austin.
- Sabaka, T. J., N. Olsen, and R. A. Langel (2000), A comprehensive model of the near-Earth magnetic field: Phase 3, *NASA Tech. Memo.*, *TM-2000-20,9894*.
- Schlenger, C. M. (1985), Magnetization of the lower crust and interpretation of regional magnetic anomalies: Example from Lofoten and Vesterålen, Norway, *J. Geophys. Res.*, *90*, 11,484–11,504.
- Schmitz, M., D. Chalbaud, J. Castillo, and C. Izarra (2002), The crustal structure of the Guayana Venezuela, from seismic refraction and gravity data, *Tectonophysics*, *345*, 103–118.
- Shive, P. N. (1989), Can remanent magnetisation in the deep crust contribute to long wavelength magnetic anomalies?, *Geophys. Res. Lett.*, *16*, 89–92.
- Shive, P. N., R. J. Blakely, B. R. Frost, and D. M. Fountain (1992), Magnetic properties of the lower continental crust, in *Continental Lower Crust*, edited by D. M. Fountain, R. Arculus, and R. W. Kay, pp. 145–177, Elsevier, New York.
- Sweeney, J. F. (1981), Arctic seafloor structure and tectonic evolution, in *Paleoreconstruction of the Continents, Geodyn. Ser.*, vol. 2, edited by M. W. McElhinny and D. A. Valencio, pp. 55–113, AGU, Washington, D. C.

- Taylor, P. T. (1991), Investigation of plate boundaries in the eastern Indian Ocean using Magsat data, *Tectonophysics*, 192, 153–158.
- Taylor, P. T., and D. N. Ravat (1995), An interpretation of the Magsat anomalies of central Europe, *J. Appl. Geophys.*, 34, 83–91.
- Taylor, S. R., and S. M. McLennan (1985), *The Continental Crust: Its Composition and Evolution*, 312 pp., Blackwell Sci., Malden, Mass.
- Toft, P. B., and J. Arkani-Hamed (1992), Magnetization of the Pacific ocean lithosphere deduced from Magsat data, *J. Geophys. Res.*, 97, 4387–4406.
- Toft, P. B., and S. E. Haggerty (1988), Limiting depth of magnetization in cratonic lithosphere, *Geophys. Res. Lett.*, 15, 530–533.
- Toft, P. B., P. T. Taylor, J. Arkani-Hamed, and S. E. Haggerty (1992), Interpretation of satellite magnetic anomalies over the West African craton, *Tectonophysics*, 212, 21–32.
- Treloar, N. A., P. N. Shive, and D. M. Fountain (1986), Viscous remanence acquisition in deep crustal rocks (abstract), *Eos Trans. AGU*, 67, 266.
- Verhoef, J., et al. (1996), Magnetic anomalies of the Arctic and North Atlantic oceans and adjacent land areas, *Geol. Surv. Can. Open File*, 3125a. (Available at <http://agcwww.bio.ns.ca/pubprod/of3125etc.html>)
- Wasilewski, P. J., and M. A. Mayhew (1992), The Moho as a magnetic boundary revisited, *Geophys. Res. Lett.*, 19, 2259–2262.
- Wessel, P., and W. H. F. Smith (1998), New, improved version of the Generic Mapping Tools Released, *Eos Trans. AGU*, 79, 579.
- Wheeler, K. A. (2003), Crustal magnetization distribution deduced from CHAMP data, in *CHAMP Mission Results I*, pp. 281–287, Springer, New York.
- White, R. S., D. McKenzie, and R. K. O’Nions (1992), Oceanic crustal thickness from seismic measurements and rare earth element inversions, *J. Geophys. Res.*, 97, 19,683–19,715.
- Worm, H. U., and C. Rolf (1994), Remanent magnetization of KTB drill cores, *Sci. Drill.*, 4, 185–196.
- Ziegler, A. M., C. R. Scotese, and S. F. Barrett (1983), Mesozoic and Cenozoic paleogeographic maps, in *Tidal Friction and the Earth Rotation II*, edited by P. Brosche and J. Sundermann, pp. 240–252, Springer, New York.

K. Hemant, GeoForschungsZentrum Potsdam, Telegrafenberg, Potsdam, D-14473 Brandenburg, Germany. (hemant@gfz-potsdam.de)

S. Maus, CIRES, University of Colorado, 325 Broadway, Boulder, CO 80305-3328, USA.